algorithms

MDPI

Article

Design of PIDD$^{\alpha}$ Controller for Robust Performance of Process Plants

Muhammad Amir Fawwaz [1], Kishore Bingi [1,*], Rosdiazli Ibrahim [1], P. Arun Mozhi Devan [1] and B. Rajanarayan Prusty [2,*]

[1] Department of Electrical and Electronics Engineering, Universiti Teknologi PETRONAS, Seri Iskandar 32610, Malaysia; fawwaz_18002231@utp.edu.my (M.A.F.); rosdiazli@utp.edu.my (R.I.); arun.selvam@utp.edu.my (P.A.M.D.)

[2] Department of Electrical, Electronics and Communication Engineering, School of Engineering, Galgotias University, Greater Noida 203201, India

* Correspondence: bingi.kishore@utp.edu.my (K.B.); b.r.prusty@ieee.org (B.R.P.)

Abstract: Managing industrial processes in real-time is challenging due to the nonlinearity and sensitivity of these processes. This unpredictability can cause delays in the regulation of these processes. The PID controller family is commonly used in these situations, but their performance is inadequate in systems and surroundings with varying set-points, longer dead times, external noises, and disturbances. Therefore, this research has developed a novel controller structure for PIDD$^{\alpha}$ that incorporates the second derivative term from PIDD^{2} while exclusively using fractional order parameters for the second derivative term. The controllers' robust performance has been evaluated on four simulation plants: first order, second order with time delay, third-order magnetic levitation systems, and fourth-order automatic voltage regulation systems. The controllers' performance has also been evaluated on experimental models of pressure and flow processes. The proposed controller exhibits the least overshoot among all the systems tested. The overshoot for the first-order systems is 9.63%, for the third-order magnetic levitation system, it is 12.82%, and for the fourth-order automatic voltage regulation system, it is only 0.19%. In the pressure process plant, the overshoot is only 4.83%. All controllers for the second-order systems have a time delay, while the flow process plant has no overshoot. The proposed controller demonstrates superior settling times in various systems. For first-order systems, the settling time is 14.26 s, while in the pressure process plant, the settling time is 8.9543 s. Similarly, the proposed controllers for the second-order system with a time delay and the flow process plant have the same settling time of 46.0495 s. In addition, the proposed controller results in the lowest rise time for three different systems. The rise time is only 0.0075 s for the third-order magnetic levitation system, while the fourth-order automatic voltage regulation system has a rise time of 0.0232 s. Finally, for the flow process plant, the proposed controller has the least rise time of 25.7819 s. Thus, in all the cases, the proposed controller results in a more robust controller structure that provides the desired performance of a regular PIDD^{2} controller, offering better dynamic responses, shorter settling times, faster rise times, and reduced overshoot. Based on the analysis, it is evident that PIDD$^{\alpha}$ outperforms both PID and FOPID control techniques due to its ability to produce a more robust control signal.

Keywords: PID; fractional order; robustness; process control; stability

Citation: Fawwaz, M.A.; Bingi, K.; Ibrahim, R.; Devan, P.A.M.; Prusty, B.R. Design of PIDD$^{\alpha}$ Controller for Robust Performance of Process Plants. *Algorithms* **2023**, *16*, 437. https://doi.org/10.3390/a16090437

Academic Editors: Quanmin Zhu, Jing Chen and Ya Gu

Received: 20 August 2023
Revised: 8 September 2023
Accepted: 8 September 2023
Published: 11 September 2023

1. Introduction

In recent years, various industries, including oil and gas, chemical manufacturing, food and beverages, and pharmaceuticals, have prioritised automating their process plants by incorporating advanced technology and software to manage and oversee industrial processes, aiming to minimise human intervention and enhance efficiency and safety. Automation is typically achieved by regulating and supervising process variables, such as

flow, temperature, level, and pressure within the process plant. PID controllers have gained popularity in automatic control systems due to their simplicity, good performance, and cost-effectiveness [1–4]. However, their effectiveness must be improved to cater to more complex and higher-order systems [5]. Recent research suggests the integration of more complex PID controller configurations, such as fractional order calculus and higher-order derivative terms, such as PIDD^2 and proportional integral derivative acceleration controllers, to regulate more complex systems [1,3,6–8]. The PIDD^2 controller has found extensive usage in power systems, power electronics, and control systems, and its recent developments and applications are discussed in the following sections. The list of abbreviations used in the following sections is available at the end of the manuscript.

1.1. Power System Applications

1.1.1. AVR Systems

Ensuring the reliability of power systems is crucial, and the automatic voltage regulator system plays a critical role in regulating the voltage of synchronous generators. However, this system is prone to insufficient oscillating transient response, maximum overshoot, additional settling time, and steady-state errors. Despite extensive research to develop a control strategy for the AVR system, finding the best approach requires significant time and effort. The authors in [1] proposed a PIDD^2 controller for the synchronous generator to enhance the system's robustness. The controller has been practically implemented and demonstrated better performance than its counterparts. An iterative procedure obtains the controller parameters through a constrained optimisation problem. A PIDD^2 controller tuned with an improved Runge Kutta optimiser has been developed to enhance the AVR systems' transient and robustness performance [9]. The controller is designed to strengthen transient and robustness performance, and simulation results showed better transient response characteristics than other controllers. Another PIDD^2 controller tuned with the coronavirus herd immunity optimiser algorithm is presented in [10] to achieve optimal system control. The practical implementation of this controller exhibited superior performance in ITAE and ISAE compared to PIDD^2 controllers tuned with other algorithms.

In control systems, optimal control is crucial to ensure efficient performance. Using a PIDD^2 controller, tuned with the Archimedes optimisation algorithm [11], has proven effective in achieving optimal control, as demonstrated in [12]. Additionally, an equilibrium optimiser has successfully optimised the design of a PIDD^2 controller for controlling an AVR system, as presented in [13]. Incorporating hybrid optimisation, considering the excitation voltage limitations of an AVR system [14], has led to the development of an optimal PIDD^2 controller from the conventional PID. Such controllers have been proposed in [12–14] and exhibited superior transient responses in comparison to alternative controllers. Further research in this field has resulted in the implementation of a hybrid algorithm consisting of simulated annealing and manta ray foraging to optimise the PIDD^2 controller, which has been shown to outperform other controllers in terms of transient response characteristics [15]. These findings highlight the significance of optimal control design in achieving desirable system performance.

In this study, a PIDD^2 controller for the AVR system is developed using whale optimisation [16]. The performance of the proposed controller design is evaluated based on transient response characteristics and compared to other controller designs and tuning algorithms, demonstrating significant improvement. Previous works, such as [7,17], have utilised particle swarm and arithmetic optimisation algorithms to tune PIDD^2 controllers for AVR systems, resulting in improved performance in all step response characteristics compared to their counterparts. Additionally, a PID controller based on a linear quadratic method is introduced for the system, which, combined with a PIDD^2 controller, demonstrated outstanding performance compared to a standard PID controller [3]. Although the PIkDND2N2 controller tuned using a coyote optimisation algorithm proposed in [18] outperformed its competitors, it had a more complex control structure due to the need to tune around seven parameters, compared to only four for PIDD^2 and five for FOPID. Recently,

a fractional-order PIDD^2 controller with optimal algorithm-tuned control parameters is proposed for the system, providing superior performance compared to all conventional controllers [19].

1.1.2. Two and Multi-Area Power System

In a two-area power system, two control areas are connected by a weak tie line. Both areas must generate enough power to meet customers' demands while maintaining the system's predetermined frequency and tie-power levels. Since frequency and active power are closely linked, the system frequency regulates any changes in power. A load frequency controller properly balances generated power and load demand. In conventional and hybrid two-area power systems, researchers in [6,20,21] have proposed a fuzzy PIDD^2 controller for voltage and frequency regulation. They have significantly improved the controller's performance compared to its counterpart in transient response characteristics by tuning the controller parameters via a gradient-based optimisation algorithm. To effectively control frequency variations in the system, the authors in [22] have proposed a design that uses a PIDD^2-PD controller for a two-area linked power system. They have simulated the proposed design by tuning controller parameters using the wild horse optimiser, and it has shown superior settling times, maximum overshoot, and undershoot values compared to other PID controllers.

In addition, a study by the authors in [23] has suggested a robust load frequency control design utilising PIDD^2. The controller's parameters are fine-tuned with the help of internal model control, which enhances the controller's transient response. Another configuration for PIDD^2 controller design is used in [24], which is applied to a two-area power system. The design is simulated and demonstrates an improvement in ISE by utilising a sine-cosine optimal algorithm. In [25], the authors introduce a PIDD controller with the 2DOF to be incorporated into a multi-area thermal system. The controller's parameters are adjusted using the cuckoo search method to improve its settling time, peak overshoot, and oscillation rate performance. The suggested design outperforms controllers like I, PI, and PID controllers.

1.2. Control System Applications

Due to their high productivity and accuracy standards, there is a growing interest in using intelligent control methods for robotic applications. Recent years have seen numerous advancements in this area, including an open–closed-loop control design using a PIDD^2/PID controller to control a robot arm, as the authors in [26] proposed. The control parameters have been improved using iterative learning control, and the design has been tested in both simulation and real-time. However, more information is needed to evaluate its performance measures and viability compared to other controller designs. Unmanned aerial vehicles, such as quadcopters, are typically flown remotely from the ground or by onboard computers. However, quadcopters have significant power efficiency limitations due to their flying stability and their four motors' constant, quick acceleration. To address this issue, a hybrid FLC-PID-PIDD^2 controller is proposed with controller parameters tuned using complementary error minimisation algorithms [27]. The simulations showed that this design outperforms other controllers, such as FLC-PID and PID controllers, regarding response time and control accuracy, making it an effective measure for enhancing stability during unmanned aerial vehicle flights.

Using magnetic levitation involves lifting or suspending a magnetic item by interacting with a magnetic field. The system requires dynamic adjustments of its electromagnets to maintain the desired position of the item. As the maglev system is naturally unstable, electronic feedback control is necessary to stabilise the levitated magnetic item. In [28], the authors proposed the PIDD^2-PID controller for a magnetic levitation system, which uses the slime mould algorithm to tune its control parameters. The simulation results of this design were compared with other controllers like ASO-FOPID, AEF-FOPID, ABC-FOPID, SCA-PID, WDO-PID, and ABC-PID controllers, and it outperformed them in terms

of performance measures. Similarly, in [2], the author proposed a method for optimal higher-order controllers, where multiple controllers such as PI2IDD2, PI2ID, PIDD^2, PID2, and PI2D are tuned with multi-objective GA algorithms. The proposed design performs better in the angular velocity's transient response and the controller's control gain. It has been observed through practical implementations that the higher-order controllers perform better than the lower-order controllers, with slight deviations in performance measures among each other.

In [4], the authors suggest using a PIDD2D3 controller for a ship power plant, which uses a digital control system simulation model and tests the proposed design's performance. The results were compared with PID and PIDD^2 controllers, and the proposed controller performed better. A marine internal combustion engine is an essential component of a ship's propulsion system that provides power. The efficiency of MICE is greatly affected by the temperature and pressure of the coolant, lubricating oil, and fuel in the engine's fuel line. The design constraints of these automated control systems come from the heat exchangers, making adjusting the temperature and pressure of lubricating oil and coolant challenging.

In [29], the PIDD^2 controller proposed by the authors for the fuel preparation system of a combustion engine outperforms the PID controller in terms of integral criterion, oscillation index, and control parameter deviation. Similarly, the controller design proposed in [30] for the hydraulic actuator, utilising a feedforward PIDD^2, is proven superior in step response compared to the PID controller. The valve-controlled hydraulic motor speed servo system, known for its quick, accurate, and efficient response due to the high-frequency response of the servo valve, is typically used in low- and medium-power applications requiring excellent accuracy. The authors in [31] have proposed a controller design utilising a feedforward PIDD^2 controller for the valve-controlled hydraulic motor system, which shows better performance in position tracking capability when simulated and compared to PID, PIDD, and differential PID controllers. It is clear from the results that the PIDD^2 controller design is a promising option for controlling various systems, providing better performance than traditional PID controllers.

Plant processes can be modelled as differential equations of varying orders, with the behaviour and order of the system being influenced by its degree of freedom and direction of motion. For instance, the transfer function of a DC motor is a second-order system, with the input voltage and shaft angle or position serving as input variables, including the armature's inductance, resulting in a third-order transfer function. To optimise predictive algorithms, the authors in [32] proposed a universal searchless method for parametric optimisation, using a PIDD^2 controller to control a third-order model with time delay. The control parameters are tuned using the universal searchless method, with simulation showing an improvement in the transient response of the set-point signal compared to the predictive PID controller.

Similarly, in [33], researchers proposed a PIDD^2 controller, tuned through a maximal stability degree method with iteration, for a second-order model with inertia and time delay. The proposed method outperforms the PID controller regarding control time and voltage overshoot, exhibiting superior performance. The authors in [34] presented a PIDD^2 controller tuned with the identification algorithm REDIC to attain adaptive self-tuning of controller parameters based on the analog model of a control plant. The proposed method significantly outperforms traditional PID controllers in terms of transient responses. Finally, in [35], researchers proposed a PIDD^2 controller for an IPDT plant model, with control parameters tuned using the quintuple real dominant pole tuning method resulting in improved performance in terms of IAE, with the proposed design surpassing PI, PID, and PIDD^2 controllers.

Diabetes mellitus is a medical condition linked to the improper control of blood glucose levels and is caused by inadequate insulin production or ineffective use of insulin in the body. Type 1 diabetes is characterised by a complete lack of insulin production, requiring a syringe or implanted micro-pump for insulin administration. Automated closed-loop devices are being explored to improve the accuracy and reliability of insulin regulation. In a recent study by the authors in [36], the FPIDD^2 controller with a two-delay differential model is proposed to simulate this scenario. The study demonstrated that this approach improved MAPE, RMSE, and insulin usage compared to other controllers, such as PD, PI, parallel PID, and single-rule-based FPID. The particle swarm optimisation algorithm enhanced performance with linearly decreasing weight, ensuring optimal results.

1.3. Power Electronic Applications

Managing output voltage in a DC-DC boost converter poses a complex challenge for control engineers. The authors in [37] have presented a PIDD^2 controller design for a non-ideal DC-DC boost converter to address this issue. The proposed method employs the IMC approach to derive the controller parameters. The practical implementation of this approach demonstrates a significant enhancement in maximum sensitivity, rise time, and total variation, surpassing the performance of its predecessor, the IMC PID controllers.

All the above literature review has been briefly summarised in Table 1. From the literature review, it can be summarized that the performance of PIDD^2 can be enhanced using the fractional-order concept. This is because fractional ordering allows for increased flexibility and robust performance [38]. Recently, a PLC-based FOPID controller has also been designed for industrial process control application [39]. From the review findings, this paper presents a novel PIDD$^\alpha$ controller that combines the advantages of FOPID controllers and PIDD controllers. The main contributions of this work are as follows:

- A new controller structure for PIDD$^\alpha$ has been proposed, which includes the second derivative term from PIDD^2 and utilizes fractional order parameters exclusively for the second derivative term.
- The controllers' robust performance has been tested in both simulation and experiment compared to PID, PIDD^2, and FOPID controllers regarding transient response characteristics.
- The controllers' robust performance has also been tested for fixed and variable set points and in the presence of external disturbances.

Table 1. Summary of recent developments and applications of PIDD^2 controller in various fields.

Ref.	Year	Controller	Parameters	Comparison	System	Tuning	Measures	Simulation/Practical	Software
[6]	2023	Fuzzy PIDD^2	8	PID, Fuzzy PID	Conventional and hybrid two-area power systems	Gradient-based optimization	ITAE	Simulation	MATLAB
[1]	2023	PIDD^2	5	PID	AVR of synchronous generator	Constrained optimization problem via an iterative procedure	IAE	Practical	MATLAB
[20]	2023	FPIDD	6	GBO tuned ID-T, FPID	Two-area hybrid system	Gradient-based optimisation	rise time, settling time, max overshoot and undershoot, ITAE	Simulation and Practical	MATLAB/Simulink
[22]	2022	PIDD^2-PD	9	PID-TID, ID-T	Two-area linked power system	Wild horse optimizer	Settling time, maximum overshoot, and undershoot values	Simulation	MATLAB/Simulink
[10]	2022	PIDD^2	4	IWO-PIDD^2, PSO-PIDD^2, OBASO-PIDD^2, ASO-PIDD^2	AVR system	Coronavirus herd immunity optimization	ITAE, ITSE	Simulation and Practical	MATLAB
[7]	2022	PIDD^2-PD	6	PIDD^2-PSO, FOPID-SMA, PID-SCA, PIDA-WOA	AVR system	Arithmetic optimisation algorithm	overshoot, rise time, settling time, phase margin, bandwidth	Simulation	MATLAB
[9]	2022	PIDD^2	6	PID, PID-F, PIDA, FOPID, PIDD^2	AVR system	Improved Runge Kutta optimiser	rise time, settling time, percent overshoot	Simulation	–
[12]	2022	PIDD^2	4	PID, FOPID, RPID, SPID	AVR system	Archimedes optimization algorithm	settling time, rise time, overshoot voltage	Simulation	–
[18]	2022	PIkDND2N2	7	FOPID, PID, PIDA, PIDD^2	AVR system	Coyote optimization algorithm	transient response and disturbance rejection	Simulation	MATLAB

Table 1. *Cont.*

Ref.	Year	Controller	Parameters	Comparison	System	Tuning	Measures	Simulation/Practical	Software
[37]	2021	PIDD^2	4	IMC PID	Non-ideal DC-DC boost converter	Internal model control	max sensitivity, rise time, total variation	Practical	MATLAB
[13]	2021	PIDD^2	6	PID, FOPID, ideal PIDD^2	AVR system	Equilibrium optimizer	rise time, settling time, overshoot	Simulation	–
[14]	2021	PIDD^2	4	SA-MRFO-PIDD^2, PSO-PIDD^2, AEO-PID	AVR system	Equilibrium optimizer-evaporation rate water cycle	rise time, delay time, overshoot	Simulation	MATLAB
[21]	2021	Fuzzy PIDD^2	5	(HSCOA, GBO, BFO)-FPIDD^2, FPID, PID	Two-area linear thermal model and linear multi-source topology in two-area environments	Gradient-based optimisation	settling time, maximum overshoot, and undershoot values	Simulation	MATLAB/Simulink
[28]	2021	PIDD^2-PID	6	(ASO, AEF, ABC)-FOPID, (SCA, WDO, ABC)-ideal PID	Magnetic levitation system	Slime mould algorithm	settling time, rise time, overshoot voltage	Simulation	MATLAB
[19]	2021	FOPIDD^2	7	FOPID, PID, PIDA, PIDD^2	AVR system	Equilibrium Optimizer	settling time, rise time, overshoot voltage	Simulation	MATLAB
[23]	2021	PIDD^2	4	PI, PID	Two-area time delayed power system model	Internal model control	Settling time, maximum overshoot and undershoot values	Simulation	MATLAB/Simulink
[15]	2021	PIDD^2	5	ideal PID, real PID, FOPID, PIDD^2	AVR system	Simulated annealing—Manta ray foraging optimization algorithm	settling time, rise time, overshoot voltage	Simulation	MATLAB

Table 1. *Cont.*

Ref.	Year	Controller	Parameters	Comparison	System	Tuning	Measures	Simulation/Practical	Software
[36]	2020	Fuzzy PIDD^2	9	PD, PI, parallel PID, and single-rule-based PID fuzzy controllers	Two-delay differential model	Particle swarm optimization with linearly decreasing weight	MAPE, RMSE, insulin used	Simulation	–
[16]	2019	PIDD^2	4	(MOL, PSO, CS, ABC)-PID	AVR system	Whale optimisation algorithm	settling time, rise time, overshoot voltage	Simulation	MATLAB/Simulink
[24]	2018	PIDD^2	7	–	Two-area power system	Sine cosine algorithm	ISE	Simulation	MATLAB/Simulink
[35]	2018	PIDD^2	4	PI, PID, PIDD^2	IPDT plant model	Quintuple real dominant poles tuning	IAE	Simulation	MATLAB/Simulink
[26]	2018	PIDD^2/PID	8	–	Neuroarm robotic manipulator	Iterative learning control	–	Simulation and Practical	–
[2]	2018	PI2IDD2, PI2ID, PIDD^2, PID2, and PI2D	3 to 5	PI2IDD2, PI2ID, PIDD^2, PID2, and PI2D	Cansat carrier launch system	Multi-objective GA	time response of angular velocity and control gain	Practical	–
[32]	2017	PIDD^2	4	predictive PID	3rd-order model with time delay	Universal search-less method	transient response of set-point signal	Simulation	–
[3]	2017	PIDD^2	4	PID tuned with DEA, PSO, ABC algorithms and LQR method	AVR system	Linear quadratic method	peak magnitude, rise time, settling time	Simulation	MATLAB
[4]	2017	PIDD^{2}D3	5	PID, PIDD^2	Ship power plant	Simulation model of a digital control system	integral index, oscillation index	Simulation	MATLAB
[29]	2017	PIDD^2	4	PID	MICE fuel preparation system	–	integral criterion, oscillation index, control parameter deviation	Simulation	MATLAB

Table 1. *Cont.*

Ref.	Year	Controller	Parameters	Comparison	System	Tuning	Measures	Simulation/Practical	Software
[27]	2017	FLC-PID-PIDD^2	4	FLC PID, PID	Unmanned aerial vehicles in indoor terrains	Complimentary error minimization algorithms	response time, control accuracy	Simulation	MATLAB/Simulink
[30]	2016	Feedforward PIDD^2	4	PID	Hydraulic continuous rotation motor electro-hydraulic servo system	–	system response	Simulation	AMESim
[25]	2015	2-DOF-PIDD	6	I, PI, PID	Multi-area thermal system	Cuckoo search algorithm	settling time, peak overshoot, oscillation rate	Simulation	MATLAB
[17]	2015	PIDD^2	4	PID, FOPID with other tuning algorithms	AVR system	Particle swarm optimization	maximum overshoot, rise time, settling time	Simulation	MATLAB
[33]	2013	PIDD^2	4	PID	2nd-order model with inertia and time delay	Maximal stability degree method with iteration	control time, overshoot	Simulation	MATLAB
[31]	2012	Feedforward PIDD^2	4	PID, PIDD, Dff-PID	Valve-controlled hydraulic motor system	–	position tracking capability	Simulation	AMESim
[34]	2003	PIDD^2	4	PID	Analogue model of control plant	Identification algorithm REDIC	transient responses	Simulation and Practical	ADAPTLAB

2. Design of Proposed PIDD$^{\alpha}$ Controller

2.1. PID Controller

The PID controllers in feedback control systems manage a system's behaviour using proportional, integral, and derivative terms. The operation of these terms is explained as follows:

- Proportional Control: This term refers to correcting action proportionate to the present error.
- Integral Control: This term is a correction based on accumulating errors over time through low-frequency compensation.
- Derivative Control: This term applies a correction based on the error's rate of change through high-frequency compensation.

The PID control action in the Laplace domain is given as follows:

$$C(s) = \frac{U(s)}{E(s)} = \frac{U(s)}{R(s) - Y(s)} = K_p + \frac{K_i}{s} + K_d s. \tag{1}$$

In the above equation, K_p, K_i, and K_d are the proportional, integral, and derivative constants. The block diagram representation of the controller is shown in Figure 1. The figure and Equation (1) show that the PID controller combines the proportional, integral, and derivative control elements to provide a composite control signal that compromises error reduction, overshoot, and oscillation mitigation. The PID controller's settings, such as the gains for each control term, can be tuned to obtain the desired performance for a particular system.

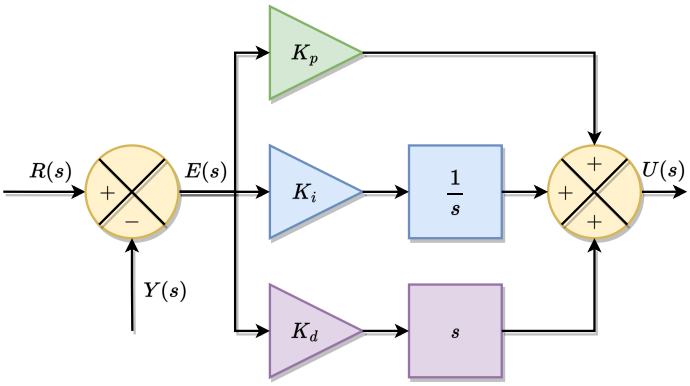

Figure 1. Block diagram of PID controller.

PID controllers can encounter problems like destabilising the system and poor performance if not tuned correctly, particularly with the integral and derivative terms. Integral windup can arise due to the integral action, causing the control action to saturate, leading to low-frequency oscillations and instability. A derivative kick can occur when the system introduces a step change to the controller, resulting in a significant spike in the derivative term as it acts upon the rate of error change [40]. It is crucial to tune the derivative term carefully as it improves the system's phase and gain margin, which can either enhance or reduce the system's stability. As a result, 80% of PID controllers used in industries have been turned off due to issues with tuning the derivative term [41].

2.2. PIDD^2 Controller

The PID with derivative filter (PIDD^2) controller is a modification of the conventional PID controller that contains an extra derivative filter. In terms of pole placement, a standard form of PID for a second-order control system is as follows:

$$C = \frac{\omega_n^2}{s^2 + 2\zeta\omega_n s + \omega_n^2}, \tag{2}$$

$$C_Z = \frac{\left(\frac{s}{\rho} + 1\right)\omega_n^2}{s^2 + 2\zeta\omega_n s + \omega_n^2} = \frac{s}{\rho}C + C, \tag{3}$$

where ω_n is the undamped natural frequency. Here, the additional derivative filter adds another zero to the transfer function where $s = -\rho$. The modified second-order controller's step response will be the original response with the scaled derivative version added based on the ρ value. The systems' response equation is shown below:

$$Y_Z = \frac{s}{\rho}Y + Y \text{ or } y_z(t) = \frac{1}{\rho}\dot{y}(t) + y(t). \tag{4}$$

As the zero located at $s = -\rho$ moves to the left side away from the origin, i.e., ρ increases, the step response will start to equate to the original step response as $y_z(t) \approx y(t)$. On the other hand, when the zero moves closer to the origin of the complex plane, i.e., ρ decreases, the effect of the derivative term becomes more apparent, causing higher overshoot and lower rise time and response time [17]. This controller design improves the phase margin, steady-state accuracy, and plant stability [9,23,28].

The PIDD^2 control action in the Laplace domain is as follows:

$$C(s) = \frac{U(s)}{E(s)} = \frac{U(s)}{R(s) - Y(s)} = K_p + \frac{K_i}{s} + K_{d1}s + K_{d2}s^2. \tag{5}$$

In the above equation, K_p, K_i, and K_{d1} are the proportional, integral, and derivative constants. K_{d2} is the constant for the extra derivative filter, which controls the smoothing of the derivative term over time. Figure 2, which shows the block diagram of the controller and Equation (5), the PIDD^2 controller adds another derivative control element to the pre-existing PID control elements where all four constants can be tuned to achieve the desired performance characteristics.

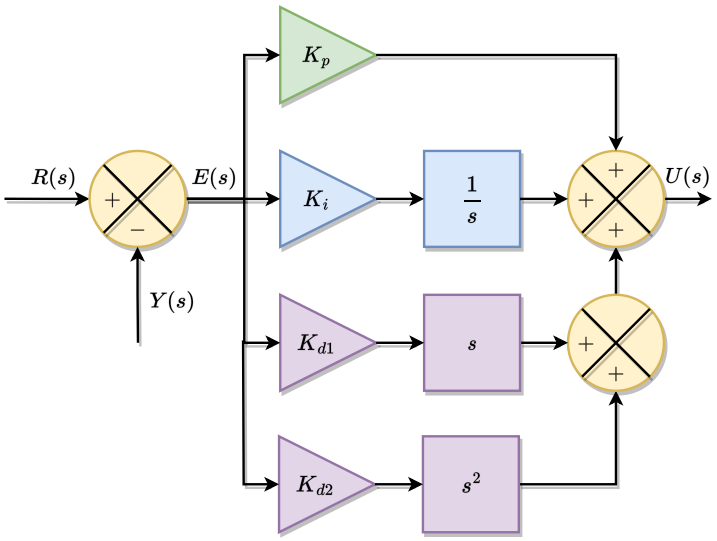

Figure 2. Block diagram of PIDD^2 controller.

This control mechanism is also subject to the derivative kick phenomenon inherent in the PID controller. In practical applications, this phenomenon can become a significant issue as its effect is amplified by the second derivative term, leading to an increase in the gain that amplifies the input signal to the square of the frequency. This is particularly problematic in high-frequency environments due to measurement noise, which can result in an overshoot in the control signal that causes the actuators to open and close abruptly, leading to wear and tear rapidly [17].

2.3. FOPID Controller

The FOPID controller utilises fractional calculus principles in its design and implementation to provide a more flexible and robust control method than traditional PID controllers. It combines non-integer orders of differentiation and integration. To comprehend frac-

tional calculus, it is essential to establish the fundamental principles and approximation techniques for resolving fractional differential equations. The differential operator, which combines fractional differentiator and integrator, is widely utilised. The equation provided below defines this operator.

$$\mathcal{D}_t^q f(t) = \begin{cases} \frac{d^q}{dt^q} f(t), & q > 0, \\ f(t), & q = 0, \\ \int_0^t f(\tau) d\tau, & q < 0, \end{cases} \tag{6}$$

where q is the fractional order.

The Riemann–Liouville definition is popular among the definitions in the literature [19,42–44]. The fractional order of order q, denoted by D^q, is given by

$$D^q[f(x)] = \frac{1}{\Gamma(n-q)} \frac{d^n}{dx^n} \int_a^x \frac{f(t)}{(x-t)^{q+1-n}} dt, \tag{7}$$

where $f(x)$ is a sufficiently well-behaved function defined on the interval $[a, b]$, n is the smallest integer greater than q, Γ is the gamma function, and $\frac{d^n}{dx^n}$ represents the nth derivative of the function with respect to x.

The Riemann–Liouville fractional derivative extends the classical derivative to non-integer orders. The integral in the definition represents the memory effect of the function $f(x)$ on its fractional derivative, where the order q determines the degree of memory.

The FOPID controller comprises proportional, integral, and derivative components that require a corresponding gain value to function effectively. The controller employs fractional-order parameters, β and μ, to adjust the integral and derivative terms, enhancing the system's stability, transient response characteristics, and robustness. The fractional integral represents the curve's projection onto a plane, with the fractional integration order acting as a weight that influences the system's responsiveness and steady-state errors [19].

$$C(s) = \frac{U(s)}{E(s)} = \frac{U(s)}{R(s) - Y(s)} = K_p + \frac{K_i}{s^\beta} + K_d s^\mu. \tag{8}$$

In the above equation, K_p, K_i, and K_{d1} are the proportional, integral, and derivative constants. The parameters β and μ represent the degree of non-integer integration and differentiation used in the controller, respectively, where $\beta > 0$ and $\mu < 2$ [43]. Figure 3 shows the block diagram for the FOPID controller where all five parameters can be tuned. Notice that a regular PID controller is achieved by setting both β and μ to be 1. By utilising non-integer values for the integral and derivative terms, the controller can simulate more complex and non-linear systems in control systems.

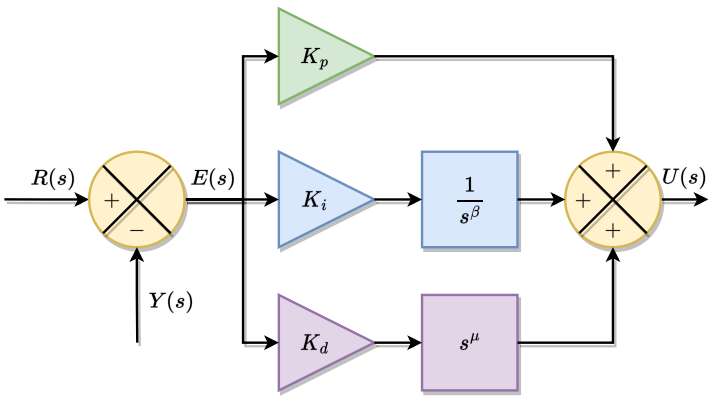

Figure 3. Block diagram of FOPID controller.

2.4. Proposed PIDD$^{\alpha}$ Controller

The configuration of the proposed PIDD$^{\alpha}$ will combine a FOPID controller and PIDD^2 controller where the fractional calculus is only implemented on the second derivative term. The proposed design is to achieve a compromise between the robustness and superior performance of the controller to handle non-linear processes through the utilisation of non-integer differentiation while also reducing the increased complexity that the FOPIDD^2 controller faced by only having five tuning parameters instead of seven.

The PIDD$^{\alpha}$ control action in Laplace's domain is given as,

$$C(s) = \frac{U(s)}{E(s)} = \frac{U(s)}{R(s) - Y(s)} = K_p + \frac{K_i}{s} + K_{d1}s + K_{d2}s^{\alpha}. \tag{9}$$

In the above equation, K_p, K_i, K_{d1}, and K_{d2} are the proportional, integral, and derivative constants. The order α represents the non-integer differentiation parameter used in the controller. Figure 4 shows the block diagram of the proposed controller where the parameters can be tuned to control both linear and non-linear processes. A PID controller can be achieved when $\alpha = 0$ and PIDD^2 controller can be achieved when $\alpha = 2$, allowing the proposed controller to control linear order and non-linear processes.

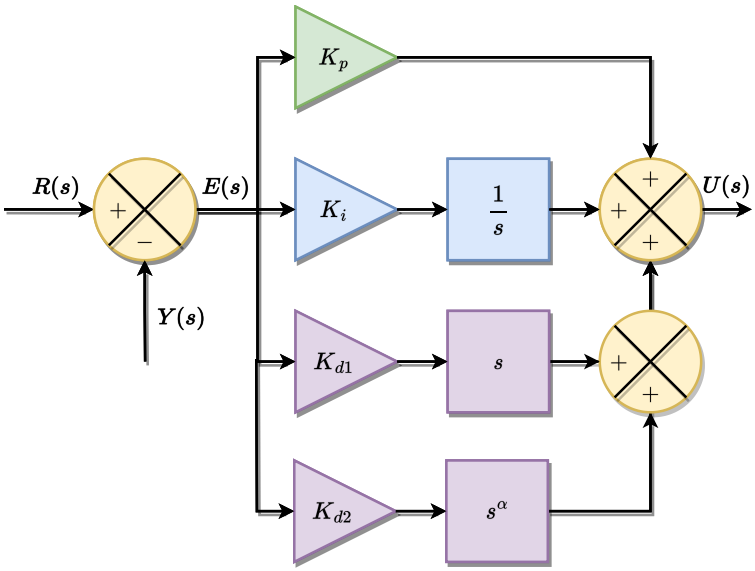

Figure 4. Block diagram of PIDD$^{\alpha}$ controller.

It is important to note that the fractional-order operators can impact the controller performance, and reliable approximation methods are available to solve these fractional-order operators. The Oustaloop method and the Matsuda method are two commonly used approximation techniques. The Matsuda method involves obtaining a rational s^{α} model through continued fraction expansion, which can create a transfer function of s^{α} by fitting the original model at desired frequency points. The order of approximation, 'N', should be an even number to avoid an improper transfer function creation [45]. On the other hand, the Oustaloop method is the most widely used method for integer-order approximation of fractional-order operators. However, it is limited in fitting the expected frequency range in practical applications [46].

3. Simulation Study

This study uses simulations to evaluate the performance of a proposed controller. The parameters used in the study are gathered from existing literature and cover various processes with different transfer functions and behaviours. The proposed controller's characteristics, such as percentage overshoot (Mp), rise time (tr), and settling time (ts),

are measured and compared to other controllers discussed in the paper, including PID, PIDD^2, and FOPID.

The controller gains are kept constant for all four controllers, except for PIDD$^\alpha$ and FOPID, which use fractional parameters obtained through Oustaloup approximation. The fractional parameters are selected through trial and error. The Oustaloup approximation's frequency range and order are $(10^{-4}, 10^4)$ and 5, respectively. The general block diagram of the considered plants is shown in Figure 5. From the figure, the transfer function of a closed-loop block diagram is computed as follows:

$$G(s) = \frac{G_p(s) \cdot C(s)}{1 + G_p(s) \cdot C(s)}, \tag{10}$$

where $G_p(s)$ and $C(s)$ are the respective transfer functions of plant and controller.

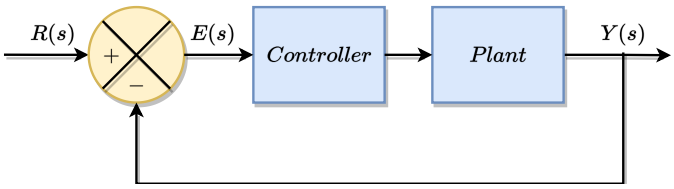

Figure 5. General block diagram of closed-loop controller with unity feedback.

3.1. First-Order System

A generic mathematical equation representing a first-order equation is selected to simulate a PID, PIDD^2, FOPID, and PIDD$^\alpha$ controlling a plant in a simulation. An RC low-pass filter circuit is an example of a real-life first-order system. To obtain the closed-loop transfer function of the entire system, Equation (10) is used with $C(s)$ substituted with Equations (1), (5), (8) and (9), and $G_p(s) = \frac{1}{5s+1}$. The controller gains, fractional parameters, and transient response characteristics used are shown in Table 2 and Figures 6–8.

Table 2. Controller parameters and transient response characteristics for first order system.

Controller	K_p	K_i	K_{d1}	K_{d2}	μ	β	α	Mp (%)	t_r (s)	t_s (s)
PID	1	1	2	–	-	–	–	20.3731	3.6417	27.4682
PIDD^2	1	1	2	1	-	–	–	22.8111	4.985	28.1916
FOPID	1	1	2	–	0.5	0.98	–	9.6332	3.8846	14.2615
PIDD$^\alpha$	1	1	2	1	–	–	0.1	11.068	3.867	14.2194

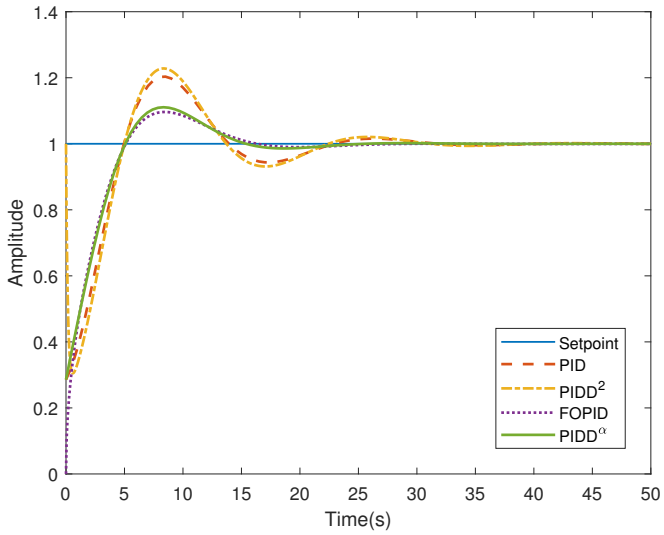

Figure 6. Step response of controller structure for first order system.

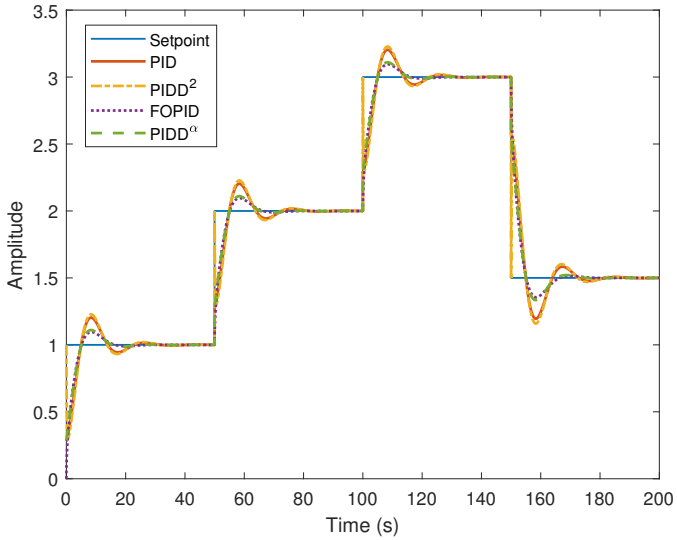

Figure 7. Variable set-point tracking of controller structure for first order system.

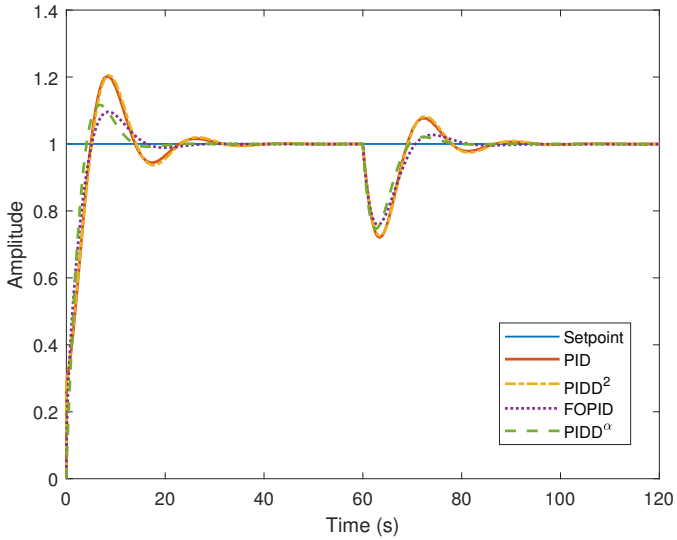

Figure 8. Disturbance rejection of controller structure for first order system.

Based on the simulation results, using fractional parameters leads to significant improvements in transient response characteristics compared to integer parameters. Both the FOPID and proposed PIDD$^\alpha$ controllers show better performance in overshoot, with 9.6332% and 11.068%, respectively, as well as in settling time, with 14.2615 s and 14.2194 s, respectively, in contrast to the PID and PIDD^2 controllers. The PID controller shows the lowest t_r of 3.6147 s, while the PIDD^2 controller performs the worst in all three transient response characteristics. Despite performing worse than FOPID in overshoots, the proposed PIDD$^\alpha$ controller outperforms the t_r of 3.867 s and settling time of 14.2194 s. Overall, the proposed PIDD$^\alpha$ controller demonstrates the best performance on average compared to its competitors.

The initial set-point is designated 1 when the time is 0 to monitor set-point tracking performance. After that, at 50 s, 100 s, and 150 s, the set-point changes to 2, 3, and 1.5, respectively. These changes cover both positive and negative changes in the controller. The set-point changes at intervals of 50 s to ensure that the step responses can reach their respective steady-state values, as specified in Table 2.

Figure 7 shows that each controller structure can manage the output to reach each set-point change. In terms of overall performance, the proposed PIDD$^{\alpha}$ controller outperforms its competitors. For disturbance rejection, a disturbance magnitude of -0.2 is introduced to the controller structure at the 60 s to replicate external disturbances that can take place in a real-world plant environment. Figure 8 illustrates that each controller structure can reject the disturbance by managing the output to reach the set-point following the step response. Overall, the proposed PIDD$^{\alpha}$ controller achieves the best overall performance compared to its competitors.

3.2. Second-Order Model with Inertia and Time Delay

The current section focuses on the model object, which is based on [33] and represents a second-order system with inertia and time delay. The block diagram of this system is comparable to the first-order plant discussed in Section 3.1. The transfer function of the model, which has a time delay of 0.2 s, is as follows:

$$G_p(s) = \frac{0.37}{1.4299s^2 + 2.46s + 1} e^{-0.2s}. \tag{11}$$

Following the methodology outlined in the preceding section, the controller parameters, transient response characteristics, step responses, and set-point tracking of various controllers have been illustrated in Table 3 and Figures 9–11. Based on the simulation results, it is clear that both PIDD^2 and the proposed PIDD$^{\alpha}$ controllers outperform PID and FOPID controllers in terms of overshoot values. Specifically, PIDD^2 achieved an impressive overshoot value of 0%, while the proposed PIDD$^{\alpha}$ achieved an overshoot value of 0.0864%.

Table 3. Controller parameters and transient response characteristics for second-order system.

Controller	K_p	K_i	K_{d1}	K_{d2}	μ	β	α	Mp (%)	t_r (s)	t_s (s)
PID	17.5	4.12	9.46	–	–	–	–	3.7692	0.3821	6.1165
PIDD^2	17.5	4.12	9.46	0.3	–	–	–	0	0.4606	6.1126
FOPID	17.5	4.12	9.46	–	1	1.2	–	2.9108	0.3869	3.1772
PIDD$^{\alpha}$	17.5	4.12	9.46	0.3	–	–	1.75	0.0864	0.4037	6.1118

In comparison, PID and FOPID controllers only managed to achieve overshoot values of 3.7692% and 2.9108%, respectively. Furthermore, the utilisation of fractional parameters in the integral control of the FOPID controller resulted in a significant reduction in the response time of the plant, from 6.11 s to 3.17 s.

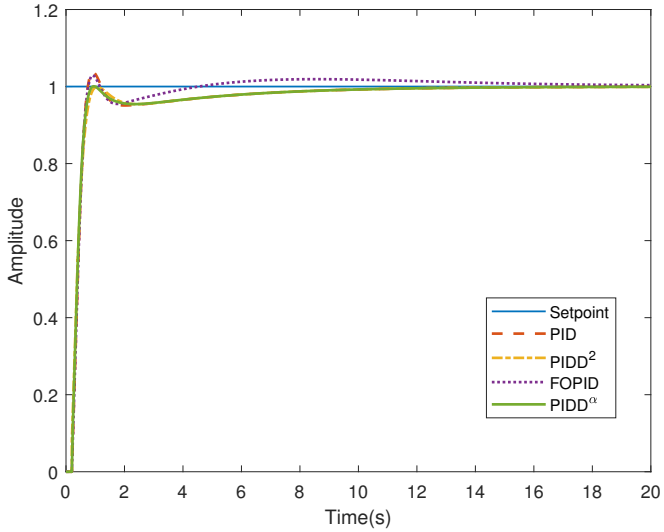

Figure 9. Step response of controller structure for second-order system.

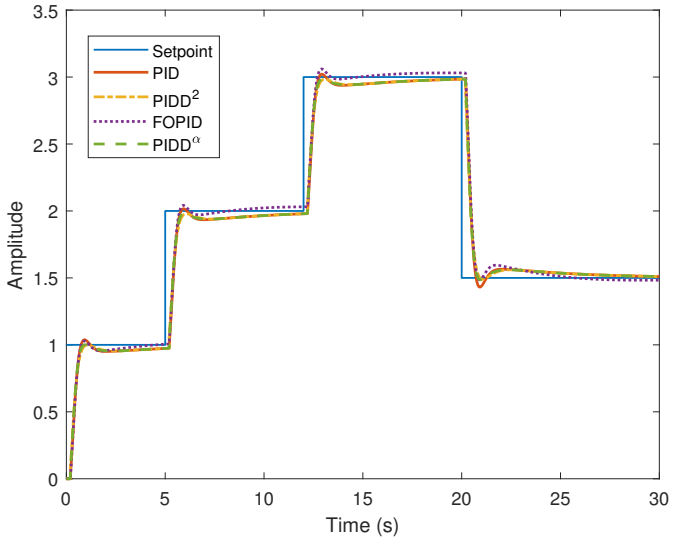

Figure 10. Variable set-point tracking of controller structure for second-order system.

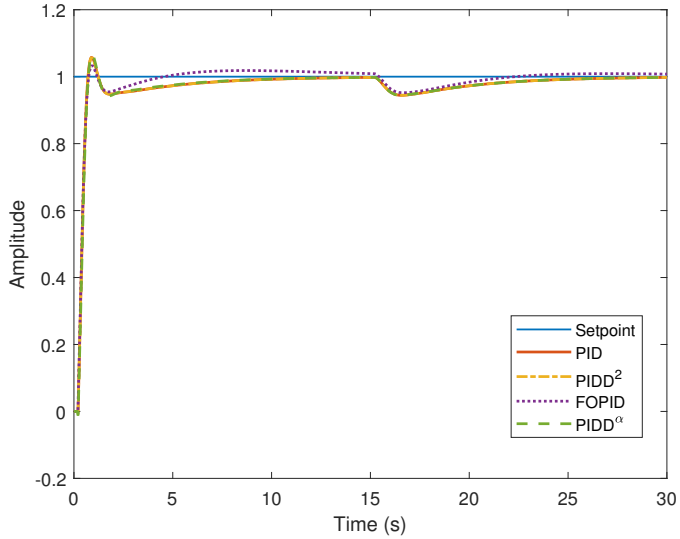

Figure 11. Disturbance rejection of controller structure for second-order system.

However, this came at the cost of a slightly increased t_r of 0.3869 s at the start of a step change and an overshoot of 2.9108%. While the PID controller had the lowest t_r of 0.3821 s, it had the highest overshoot value of 3.7692% among all the other controllers. On the other hand, the PIDD^2 controller managed to achieve an impressive overshoot value of 0%, but at the expense of a higher t_r of 0.4606 s. Overall, the proposed controller demonstrated the best overall performance when compared to the other controllers, achieving a lower t_r of 0.4037 s and t_s of 6.1118 s compared to the PIDD^2 controller, with only a slight increase in overshoot of 0.0864%.

During the tracking performance, the set-point changes to 2, 3, and 1.5 at 5 s, 12 s, and 20 s, respectively, encompassing both positive and negative changes occurring in the controller as illustrated in Figure 10. The intervals of the set-point changes are precisely planned to ensure that the step responses can attain their steady-state values, which are tabulated in Table 3.

Here, each controller structure can control the output for achieving each set-point change following the step response. The proposed PIDD$^\alpha$ controller outperforms its competitors, delivering the best overall performance. Further, to simulate plant behaviour where

external disturbances occur, a disturbance magnitude of -0.2 is introduced to the controller structure at 15 s for disturbance rejection. Figure 11 demonstrates that each controller structure can reject the disturbance by controlling the output to attain the set-point following the step response. The proposed PIDD$^{\alpha}$ controller stands out from its competitors, delivering the best overall performance.

3.3. Magnetic Levitation System

A magnetic levitation system from authors of [28] is used as the plant for this system. The control is performed with an input voltage, which controls the current flowing through the electromagnet, which in turn manipulates the height of the ball to levitate. To ensure that the ball levitates in place, the overshoot of the control system must be low and closest to the desired height. The magnetic levitation system can be represented as a transfer function given as

$$G_p(s) = \frac{885.9}{s^3 + 100s^2 - 19.62s - 1962}. \tag{12}$$

The open-loop response of the plant in Figure 12 shows that the system is unstable, which means the ball may fall off the system.

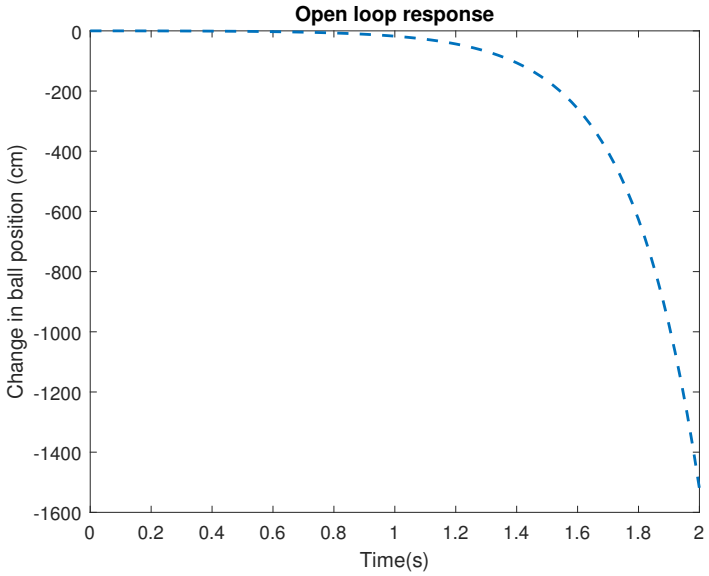

Figure 12. Open-loop response of magnetic levitation system.

To control the system and to reach stability, the plant is controlled by all four controllers, similar to previous sections where the controller parameters, transient response characteristics, and step response are shown in Table 4 and Figure 13.

Table 4. Controller parameters and transient response characteristics for magnetic levitation system.

Controller	K_p	K_i	K_{d1}	K_{d2}	μ	β	α	Mp (%)	t_r (s)	t_s (s)
PID	-159	-139	-8	–	–	–	–	44.5024	0.0167	0.1723
PIDD^2	-159	-139	-8	-0.18	–	–	–	13.0223	0.0207	0.1914
FOPID	-159	-139	-8	–	0.9	1.1	–	35.1198	0.0128	0.1989
PIDD$^{\alpha}$	-159	-139	-8	-0.18	–	–	2.04	12.8299	0.0075	0.2025

Achieving set-point tracking involves changing the set-point from 1 to 2, 3, and 1.5 at 0.3 s, 0.6 s, and 0.9 s, respectively, and their numerical analysis is listed in Table 4. Figure 14 shows that each controller structure successfully controls the output to reach each set-point change following the step response.

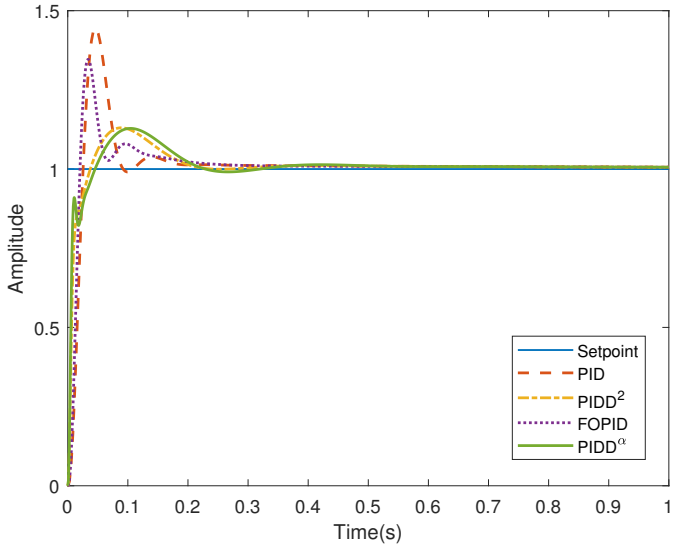

Figure 13. Step response of controller structure for magnetic levitation system.

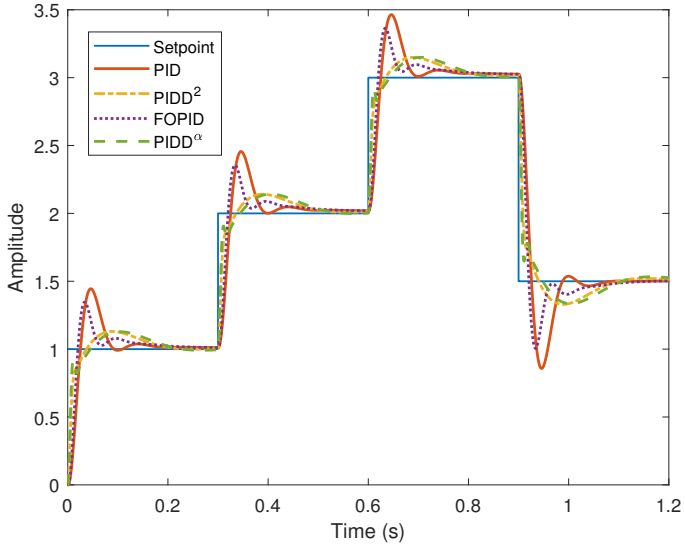

Figure 14. Variable set-point tracking of controller structure for magnetic levitation system.

Among its competitors, the proposed PIDD$^\alpha$ controller performs the best in achieving the desired outcome. A disturbance magnitude of -12 is introduced to the controller structure at 0.4 s to emulate real-world behaviour. This disturbance represents external disturbances that can occur in the overall process plant. Figure 15 shows that each controller structure can successfully reject the disturbance by controlling the output to reach the set-point following the step response. Once again, the proposed PIDD$^\alpha$ controller outperforms its competitors in achieving the desired performance.

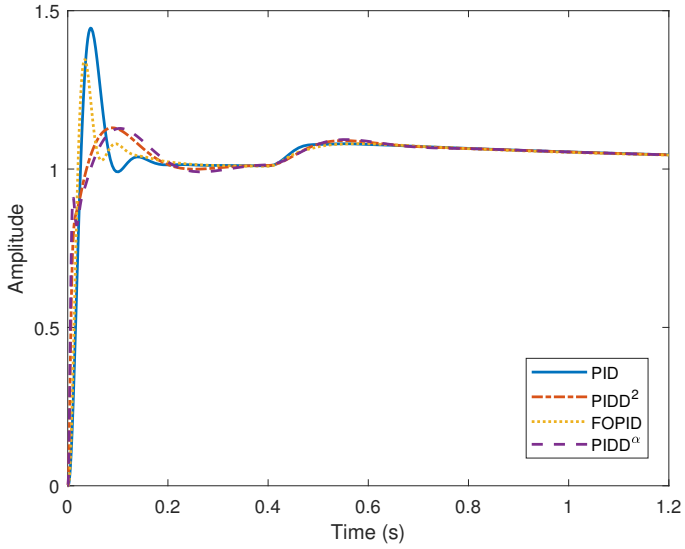

Figure 15. Disturbance rejection of controller structure for magnetic levitation system.

3.4. Automatic Voltage Regulation System

The AVR system regulates the terminal voltage of a generator to a predetermined nominal value by using a sensor located at the generator's output, which measures the actual value, calculates the error signal, and sends it back to the controller. The controller then sends a control signal to the amplifier, exciter, and generator, correcting the output voltage [13]. The AVR system can be represented as a transfer function given by the following equation:

$$G_p(s) = \frac{0.1s + 10}{0.0004s^4 + 0.045s^3 + 0.555s^2 + 1.51s + 11}. \tag{13}$$

The system response in Figure 16 shows that it is a stable system, although it reaches a steady state at around 10 s and suffers tremendous overshoot values. So, the control action must be able to reduce the overshoot value, rise time, and settling time to achieve its objective. All four controllers control the plant, similar to previous sections where the controller parameters, transient response characteristics, and step response are shown in Table 5 and Figure 17.

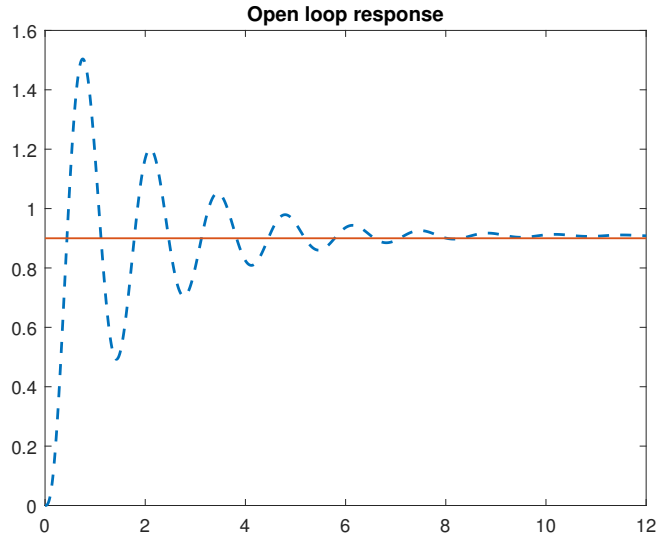

Figure 16. Open-loop response of an AVR system.

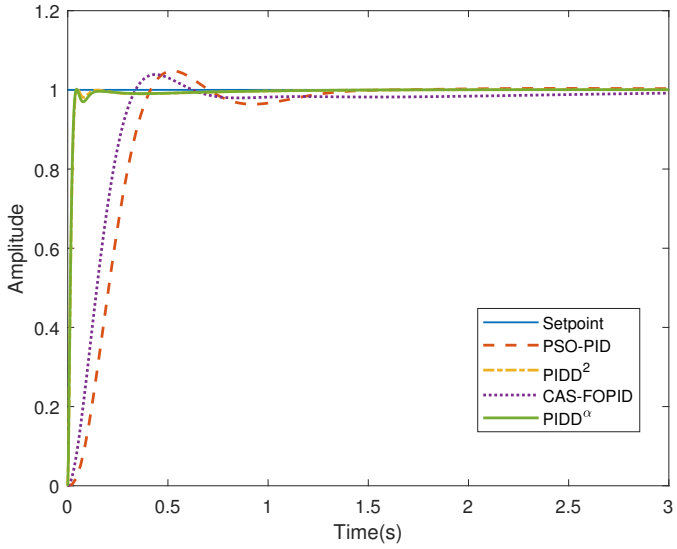

Figure 17. Step response of controller structure for an AVR system.

Table 5. Controller parameters and transient response characteristics for an AVR system.

Controller	K_p	K_i	K_{d1}	K_{d2}	μ	β	α	Mp (%)	t_r (s)	t_s (s)
PID	4.8938	3.2301	2.2479	-	-	-	-	4.7876	0.2582	1.1458
PIDD^2	4.8938	3.2301	2.2479	0.2048	-	-	-	0.2872	0.0245	0.0373
FOPID	4.8938	3.2301	2.2479	-	1.1122	1.0624	-	3.8758	0.2196	0.9012
PIDD$^\alpha$	4.8938	3.2301	2.2479	0.2048	–	–	2.01	0.1923	0.0232	0.0984

From the simulation results, the PIDD^2 controller and the proposed PIDD$^\alpha$ controller exhibit superior performance in all three transient response characteristics. Regarding overshoot performances, PIDD^2 and PIDD$^\alpha$ trump their competitors with values of 0.2782% and 0.1923% compared to PID and FOPID, with values of 4.7876% and 3.8753%, respectively. The same is true for t_r, where PIDD^2 and PIDD$^\alpha$ achieve 0.0245 s and 0.0232 s compared to 0.2582 s and 0.2196 s for PID and FOPID. For settling time, PIDD^2 and PIDD$^\alpha$ achieved 0.0373 s and 0.0984 s, respectively, compared to the 1.1458 s and 0.9012 s that PID and FOPID achieved. The proposed controller performs better between PIDD^2 and the proposed PIDD$^\alpha$ controller with the most negligible overshoot value and t_r of 0.1923% and 0.0232 s but at a higher t_s of 0.0984 s.

The set-point is initially set to 1, then changes to 2, 3, and 1.5 at 2 s, 4 s, and 6 s, respectively. These timed set-point changes ensure that step responses can reach their respective steady-state values. Each controller structure in Figure 18 can effectively control the output to reach the set-point changes. Regarding disturbance rejection, a disturbance magnitude of -0.3 is introduced to the controller structure at 2 s to simulate real-world plant behaviour. Figure 19 shows that each controller structure can reject the disturbance by effectively controlling the output to reach the set-point following the step response. The proposed PIDD$^\alpha$ controller outperforms competitors, delivering the best set-point tracking and disturbance rejection performance.

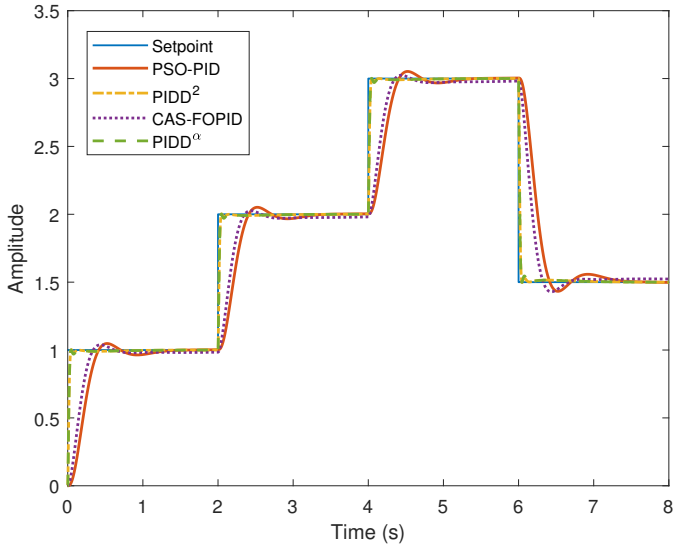

Figure 18. Variable set-point tracking of controller structure for an AVR system with PSO-PID and CAS-FOPID.

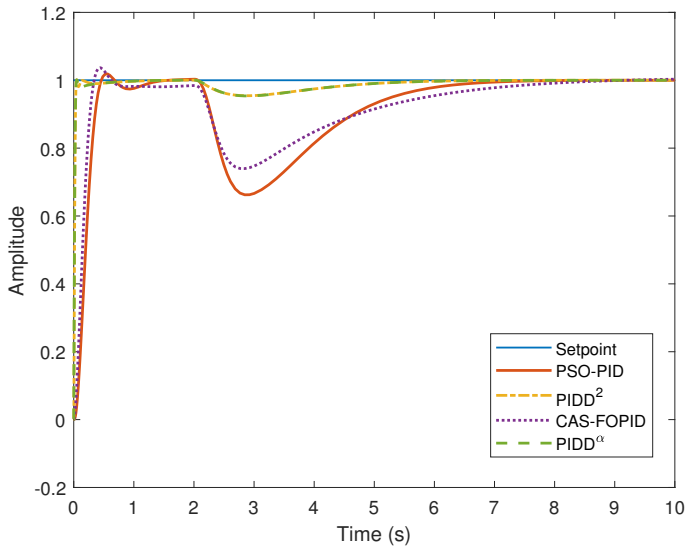

Figure 19. Disturbance rejection of controller structure for an AVR system with PSO-PID and CAS-FOPID.

4. Experimental Study

The present study applies the proposed controllers to an experimental analysis by incorporating real-time process plants available at Universiti Teknologi PETRONAS' plant process control systems laboratory. Specifically, this section delves into the schematics and operations of two such plants. Notably, a first-order transfer function with a time delay characterises both plants. However, this time delay causes the system to become non-causal and unstable. Pade approximation is used to estimate the time delay to avoid these issues. This makes the system causal and stable, making it suitable for implementing the proposed control strategies. As discussed below, these approximated transfer functions are used in the implementation process.

4.1. Real-Time Pressure Process Plant

The schematics of the real-time pressure process plant, which runs in real time, are shown in Figure 20. VL 202, the primary buffer tank, is designed to sustain up to 10 Bar of pressure from the centralised air compression system that provides it with air.

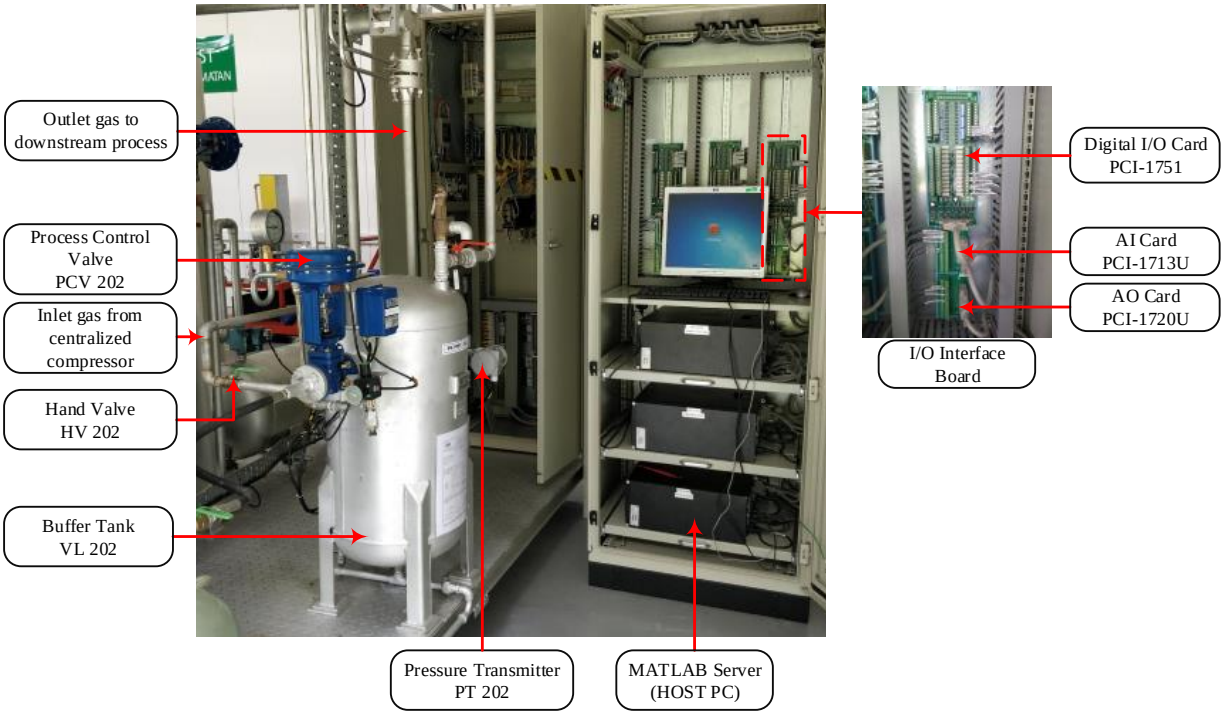

Figure 20. Schematic of real-time pressure process plant.

The pressure inside the tank can be controlled using the hand valve, HV 202, while the process control valve, PCV 202, ensures that the pressure remains constant at the desired level. The pressure is measured using pressure transmitter PT 202, converted to digital voltage values ranging from 0 to 5 V. These signals are sent to the PCV 202 pressure-indicating controller, which sends the control signal to the host PC through I/O interface boards. An analogue pressure gauge that indicates pressure fluctuations inside the tank is provided for safety. If the valve PCV 202 malfunctions, a hand-operated valve at the bottom of the buffer tank releases compressed air from the VL 202 in an emergency. The hand valve can also be employed as an external disturbance injection channel during the experiment. Excess air is released through an exit on the top of the process tank, connected to another process control valve, PCV 203, to adjust the pressure inside the buffer tank. During the experiment, this valve is kept at 50% open to prevent excessive pressure buildup inside the VL 202. The host PC sends signals to the control valve actuator PCV 202 based on the set-point value.

Figure 21 depicts the pressure process plant's P&ID diagram. The facility runs in "Remote Desktop Connection" mode for safety, with processes controlled from the central control centre. PCI cards connect the mainframe PC and field equipment, such as the control valve actuator, flow sensors, and pressure transmitter. These cards provide 2500 V DC isolation protection between PCI bus outputs.

A 32-channel analogue input board dubbed PCI-1713U receives the process plant's analogue input. It features a 12-bit resolution and a sampling rate of 100,000 samples per second. A critical component of the PCI card, the PCI-1720U module, utilises a high-quality 12-bit, 4-channel analogue output port to transfer accurate control signals to the host PC. Furthermore, with 48 bits of parallel digital input/output, the PCI-1751 card enables remote management of the pressure process plant by transmitting digital signals from the PT 202 to the host PC.

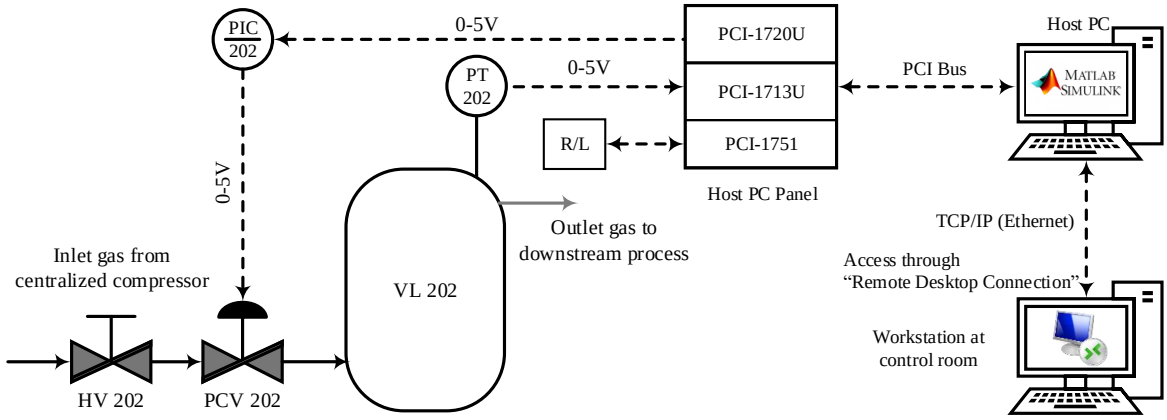

Figure 21. P&ID of the pressure process plant.

The transfer function of the pressure process plant can be derived from the open-loop response of the plant in Figure 22. Thus, the computed transfer function is given as

$$G(s) = \frac{0.866}{1.365s + 1} e^{-s} \tag{14}$$

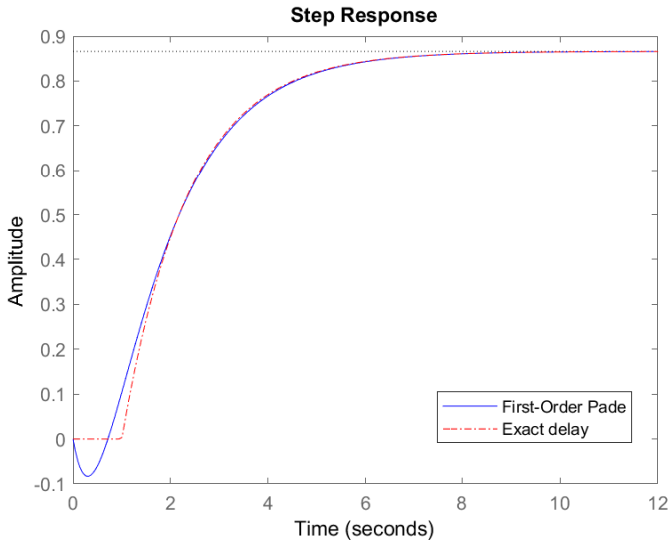

Figure 22. Open-loop response of pressure process plant before and after Pade approximation.

To control the system to reach stability, the plant is controlled by all four controllers, similar in previous systems where the following controller parameters, transient response characteristics, and step response are shown in Table 6, Figures 23–25.

Table 6. Controller parameters and transient response characteristics for real-time pressure process plant.

Controller	K_p	K_i	K_{d1}	K_{d2}	μ	β	α	Mp (%)	t_r (s)	t_s (s)
PID	0.5	0.5	−0.01	-	-	-	-	6.2148	2.8287	9.2664
PIDD^2	0.5	0.5	−0.01	−0.1	-	-	-	5.1179	2.8486	9.0571
FOPID	0.5	0.5	−0.01	-	0.99	0.15	-	5.5126	2.8792	8.96
PIDD$^\alpha$	0.5	0.5	−0.01	−0.1	-	-	1.7	4.838	2.6272	8.9543

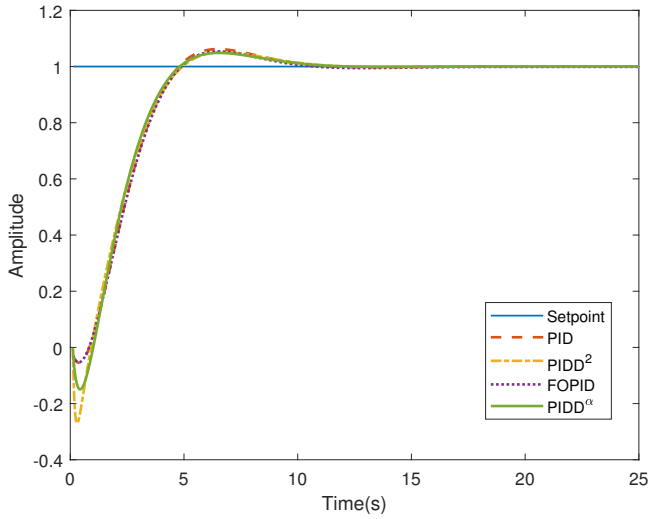

Figure 23. Step response of controller structure for pressure process plant.

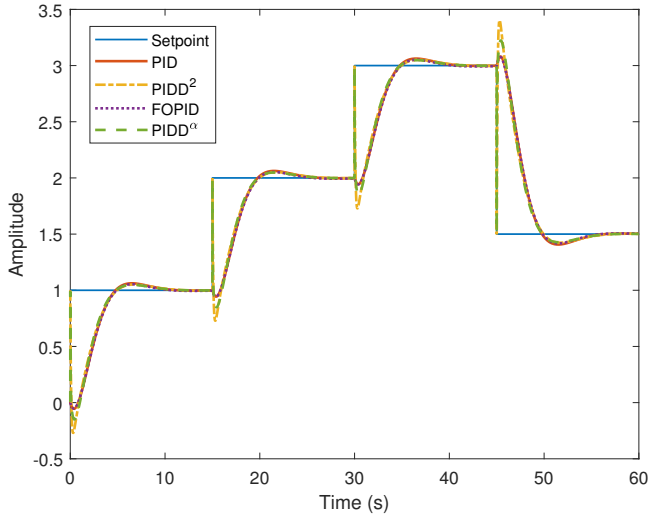

Figure 24. Variable set-point tracking of controller structure for pressure process plant.

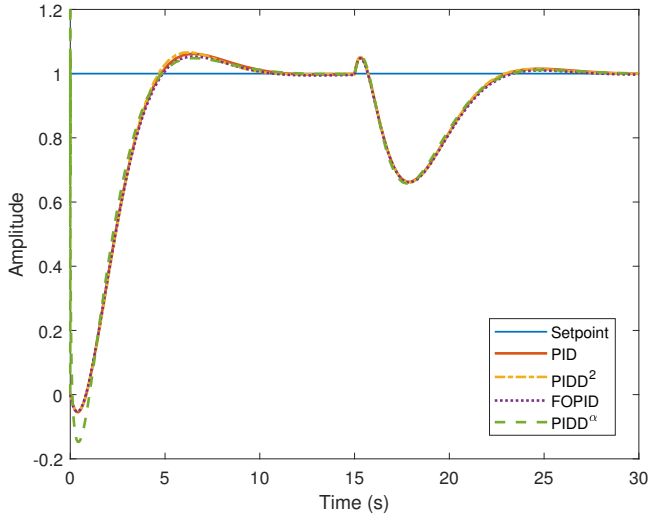

Figure 25. Disturbance rejection of controller structure for pressure process plant.

From the simulation results, PIDD2 and the proposed PIDD$^{\alpha}$ controllers have better overshoot values than PID and FOPID controllers. The proposed PIDD$^{\alpha}$ performs best with only 4.838% overshoot, while PID and FOPID controllers have 6.2148% and 5.5126%, respectively. The proposed PIDD$^{\alpha}$ also has the best rise time of 2.6272 s compared to PID, PIDD^{2}, and FOPID controllers, with rise times of 2.8287 s, 2.8486 s, and 2.8792 s, respectively. Moreover, the proposed PIDD$^{\alpha}$ outperforms its competitors in settling time with a value of 8.9543 s compared to PID, PIDD^{2}, and FOPID with values of 9.2664 s, 9.0571 s, and 8.96 s, respectively.

In the set-point tracking, the initial set-point starts at one at zero seconds and changes to 2, 3, and 1.5 at 15 s, 30 s, and 45 s, respectively. These changes cover both positive and negative changes in the controller. All set-point changes reach their steady-state values, as shown in Table 6. Figure 24 illustrates that each controller structure can achieve each set-point change following the step response. For disturbance rejection, a disturbance with a magnitude of -0.6 is introduced into the controller structure at 15 s to simulate real-world plant behaviour. Figure 25 shows that each controller structure can reject the disturbance and control the output to reach the set-point following the step response. The proposed PIDD$^{\alpha}$ controller achieves the best overall performance compared to its competitors.

4.2. Real-Time Flow Process Plant

The schematics of the real-time flow process plant are displayed in Figure 26. The process tank, VE 420, can hold up to 100 L of liquid from the product tank, VE 410, thanks to the assistance of a centrifugal pump P412. The tank's level can be adjusted using the hand valve, HV 420, while the process control valve, FCV 413, maintains a constant flow rate at the desired level. The pressure transmitter FT 413 measures the flow rate, converted into digital voltage values ranging from 0 to 5 volts. These values are then sent to the FIC 413 via a pressure-indicating controller, which sends the control signal to the host PC through I/O interface boards.

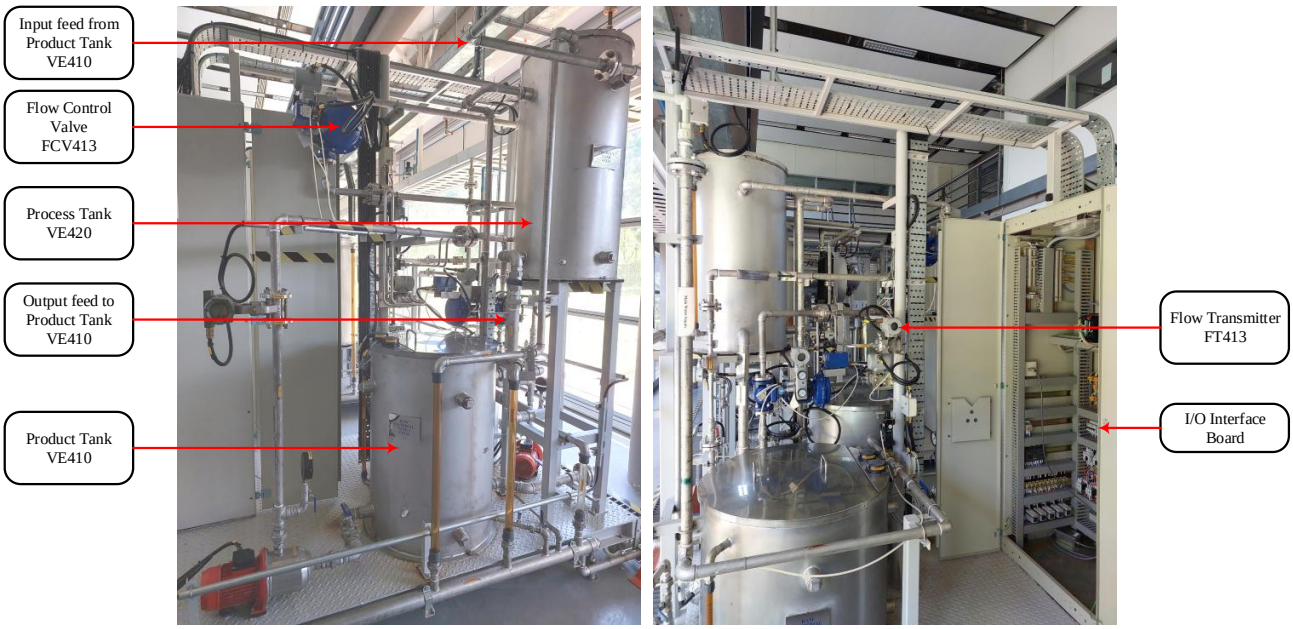

Figure 26. Schematic of real-time flow process plant.

Figure 27 illustrates the real-time flow process P&ID. The facility operates similarly to the previous pressure process plant, running in "Remote Desktop Connection" mode with PCI cards connecting the field instruments and the remote workstation.

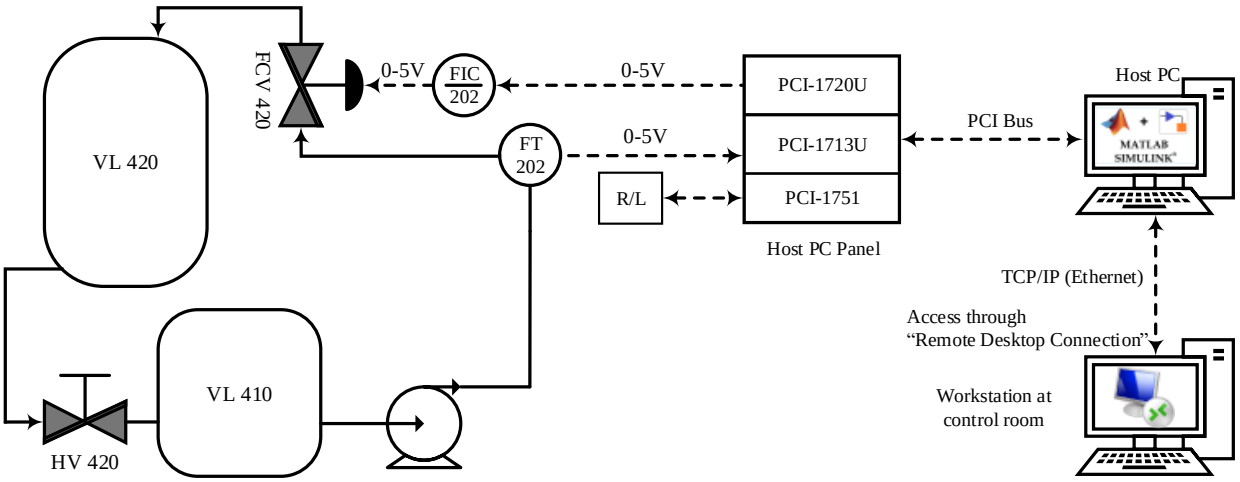

Figure 27. P&ID of the flow process plant.

The transfer function of the pressure process plant can be derived from the open-loop response of the plant in Figure 28.

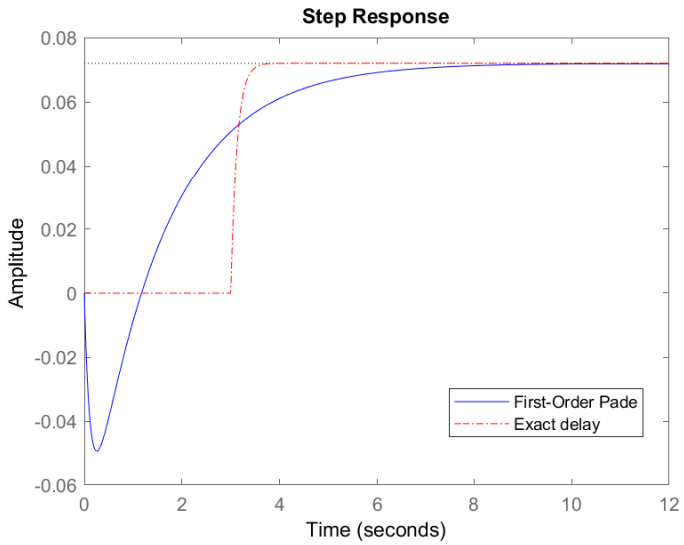

Figure 28. Open-loop response of flow process plant before and after Pade approximation.

Thus, the computed transfer function is given as

$$G(s) = \frac{0.072}{0.126s + 1} e^{-3s} \tag{15}$$

Four controllers control the plant, and these controllers have similar parameters, transient response characteristics, and step response as previous systems. The controller parameters and transient response characteristics for the real-time flow process plant are given in Table 7.

Table 7. Controller parameters and transient response characteristics for real-time flow process plant.

Controller	K_p	K_i	K_{d1}	K_{d2}	μ	β	α	Mp (%)	t_r (s)	t_s (s)
PID	1	1	0.1	-	-	-	-	0	25.8559	46.788
PIDD^2	1	1	0.1	-0.01	-	-	-	0	25.8284	46.2981
FOPID	1	1	0.1	-	0.99	0.1	-	0	27.2797	50.6053
PIDD$^\alpha$	1	1	0.1	-0.01	-	-	2.05	0	25.7819	46.0495

In Figure 29, the simulation results for set-point tracking performance indicate that all controllers have achieved 0% overshoot. However, regarding rise time, the proposed PIDD$^{\alpha}$ controller outperforms the PID and PIDD2 controllers with a time of 25.7819 s compared to 25.8559 s and 25.8284 s, respectively. The FOPID controller has the worst rise time at 27.2797 s. The same trend can be seen in settling time, where the PIDD$^{\alpha}$ controller performs better than its competitors with a time of 46.0495 s compared to the PID, PIDD2, and FOPID controllers with times of 46.788 s, 46.2981 s, and 50.6053 s, respectively.

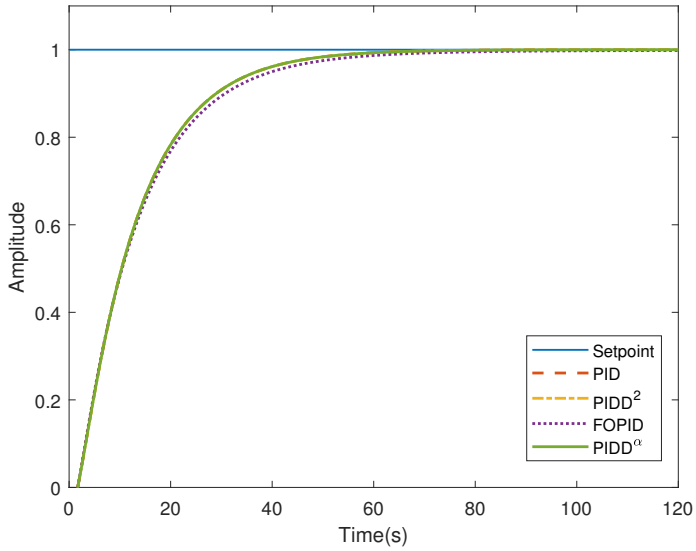

Figure 29. Step response of controller structure for flow process plant.

The process of variable set-point tracking involves changes to 2, 3, and 1.5 at 100 s, 200 s, and 300 s, respectively, from the initial value of 1 at zero seconds. These changes cover both positive and negative changes in the controller. The intervals between these changes ensure that the step responses reach their respective steady-state values, as noted in Table 7. Figure 30 shows that each controller structure can control the output to reach every set-point change following the step response.

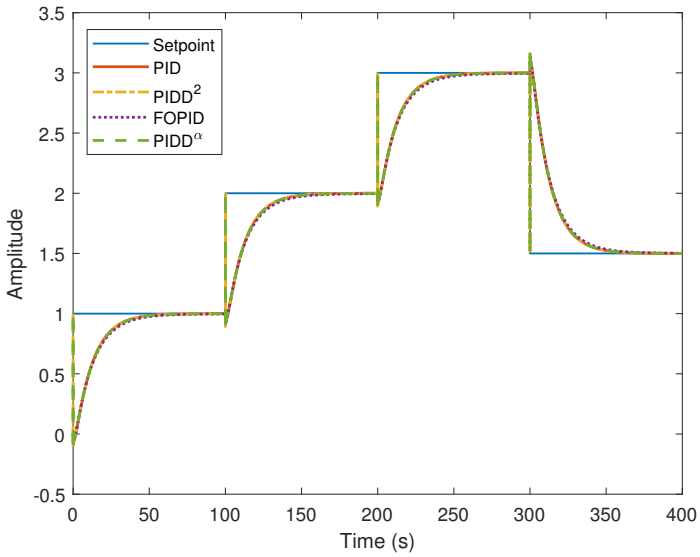

Figure 30. Variable set-point tracking of controller structure for flow process plant.

A disturbance magnitude of −1.2 is introduced to the controller structure at 100 s for disturbance rejection to simulate real-world plant behaviour when external disturbances

affect the overall process plant. Figure 31 demonstrates that each controller structure can control the output to achieve the set-point and reject the disturbance, as shown in the step response. The PIDD$^{\alpha}$ controller proposed in this study exhibits the best overall performance compared to its competitors.

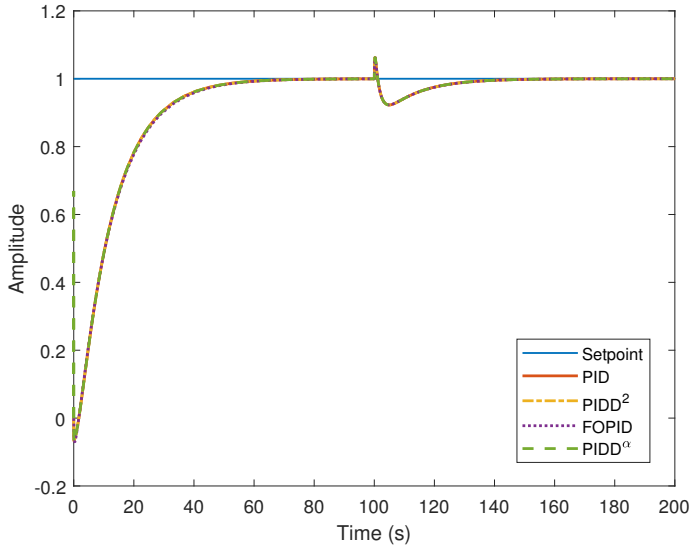

Figure 31. Disturbance rejection of controller structure for flow process plant.

5. Conclusions

This research proposes a new controller structure for PIDD$^{\alpha}$, which includes the second derivative term from PIDD^2 and utilizes fractional order parameters exclusively for the second derivative term. The controller has shown robust performance while tested in both simulation and experiment compared to PID, PIDD^2, and FOPID controllers regarding transient response characteristics. The controllers' robust performance is also tested for fixed and variable set points and in the presence of external disturbances. In all the cases, the controller gain's parameters were chosen based on literature reviews, while the fractional order parameters were determined through trial and error. The proposed controllers have been evaluated for various systems, and the results indicate their superior performance in overshoot and settling time. The proposed controllers show better performance for the first-order system, with an overshoot of 9.6332% and a settling time of 14.2615 s. Similarly, the proposed and FOPID controllers exhibit the least overshoot for the second-order system of 0.0864% and 0%, respectively. The magnetic levitation system performs better with the proposed controller, which has the least overshoot and rise time of 12.8299% and 0.0075 s, respectively. In the case of the automatic voltage regulator system, the proposed controller also outperforms the others with the least overshoot and rise time of 0.1923% and 0.0232 s, respectively. The proposed controller for the pressure process plant has the least overshoot, rise time, and settling time of 4.838%, 2.6272 s, and 8.9543 s, respectively. On the other hand, all controllers for the flow process plant have 0% overshoot, but the proposed controller has the least rise time and settling time of 25.7819 s and 46.0495 s, respectively. For all the six considered process plants, the proposed controller achieved better dynamic responses, shorter settling times, faster rise times, and reduced overshoot. This research also highlights that selecting fractional-order parameters using trial and error is inadequate. Thus, future recommendations include utilizing the tuning algorithms covered in the literature review to enhance the controller's performance and implementing the proposed controller for other control loop operations, such as feedforward and cascade control loops.

Author Contributions: Conceptualization, K.B. and R.I.; methodology, M.A.F. and R.I.; software, M.A.F.; validation, M.A.F., K.B. and P.A.M.D.; formal analysis, M.A.F. and P.A.M.D.; investigation, M.A.F. and P.A.M.D.; resources, K.B. and B.R.P.; data curation, M.A.F. and P.A.M.D.; writing—original draft preparation, M.A.F. and P.A.M.D.; writing—review and editing, K.B. and B.R.P.; visualization, K.B. and B.R.P.; supervision, K.B. and R.I.; project administration, K.B.; funding acquisition, K.B. All authors have read and agreed to the published version of the manuscript.

Funding: This research was funded by Short-Term Internal Research Funding (STIRF) with grant number 015LA0-048.

Institutional Review Board Statement: Not applicable.

Informed Consent Statement: Not applicable.

Data Availability Statement: No new data were created or analyzed in this study. Data sharing is not applicable to this article.

Conflicts of Interest: The authors declare no conflict of interest.

Abbreviations

The following abbreviations are used in this manuscript:

ABC	Artificial Bee Colony
AEF	Artificial Electric Field
ASO	Atom Search Optimization
AVR	Automatic Voltage Regulator
DOF	Degree of Freedom
FLC	Fuzzy Logic Control
FOPID	Fractional-order Proportional Integral Derivative
FPID	Fuzzy PID
FPIDD	Fuzzy Proportional-Integral-Derivative-Double Derivative
GA	Genetic Algorithm
GBO	Gradient-Based Optimization
IAE	Integral Absolute Error
IMC	Internal Model Control
ISAE	Integral Square Absolute Error
ISE	Integral Square Error
ITAE	Integral Time Absolute Error
ITSE	Integral Time Square Error
MAPE	Mean Absolute Percentage Error
MICE	Marine Internal Combustion Engines
P&ID	Piping and Instrumentation Diagram
PCI	Peripheral Interface Cards
PCV	Process Control Valve
PI	Proportional Integral
PID	Proportional Integral Derivative
PIDA	Proportional-Integral-Derivative-Acceleration
PIDD2	PID with Derivative Filter
PSO	Particle Swarm Optimization
PT	Pressure Transmitter
RMSE	Root Mean Square Error
SCA	Sine Cosine Algorithm
WDO	Wind-Driven Optimization

References

1. Veinović, S.; Stojić, D.; Ivanović, L. Optimized PIDD2 controller for AVR systems regarding robustness. *Int. J. Electr. Power Energy Syst.* **2023**, *145*, 108646. [CrossRef]
2. Jahanshahi, H.; Sari, N.N.; Pham, V.T.; Alsaadi, F.E.; Hayat, T. Optimal adaptive higher order controllers subject to sliding modes for a carrier system. *Int. J. Adv. Robot. Syst.* **2018**, *15*, 1729881418782097. [CrossRef]

3. Chatterjee, S.; Mukherjee, V. Comparative performance analysis of classical controllers for automatic voltage regulator. In Proceedings of the 2017 7th International Conference on Power Systems (ICPS), Pune, India, 21–23 December 2017; pp. 296–301.
4. Simanenkov, A.; Rozhkov, S.; Borisova, V. An algorithm of optimal settings for PIDD 2 D 3-controllers in ship power plant. In Proceedings of the 2017 IEEE 37th International Conference on Electronics and Nanotechnology (ELNANO), Kyiv, Ukraine, 18–20 April 2017; pp. 152–155.
5. Devan, P.A.M.; Ibrahim, R.; Omar, M.B.; Bingi, K.; Abdulrab, H.; Hussin, F.A. Improved Whale Optimization Algorithm for Optimal Network Coverage in Industrial Wireless Sensor Networks. In Proceedings of the 2022 International Conference on Future Trends in Smart Communities (ICFTSC), Kuching, Malaysia, 1–2 December 2022; pp. 124–129.
6. AboRas, K.M.; Ragab, M.; Shouran, M.; Alghamdi, S.; Kotb, H. Voltage and frequency regulation in smart grids via a unique Fuzzy PIDD2 controller optimized by Gradient-Based Optimization algorithm. *Energy Rep.* **2023**, *9*, 1201–1235. [CrossRef]
7. Izci, D.; Ekinci, S.; Çetin, H. Arithmetic Optimization Algorithm based Controller Design for Automatic Voltage Regulator System. In Proceedings of the 2022 Innovations in Intelligent Systems and Applications Conference (ASYU), Antalya, Turkey, 7–9 September 2022; pp. 1–5.
8. Devan, P.A.M.; Ibrahim, R.; Omar, M.; Bingi, K.; Abdulrab, H. A Novel Hybrid Harris Hawk-Arithmetic Optimization Algorithm for Industrial Wireless Mesh Networks. *Sensors* **2023**, *23*, 6224. [CrossRef]
9. Izci, D.; Ekinci, S. An improved RUN optimizer based real PID plus second-order derivative controller design as a novel method to enhance transient response and robustness of an automatic voltage regulator. *e-Prime-Adv. Electr. Eng. Electron. Energy* **2022**, *2*, 100071. [CrossRef]
10. Emiroglu, S.; Gümüş, T.E. Optimal Control of Automatic Voltage Regulator System with Coronavirus Herd Immunity Optimizer Algorithm-Based PID plus Second Order Derivative Controller. *Acad. Platf. J. Eng. Smart Syst.* **2022**, *10*, 174–183. [CrossRef]
11. Omar, M.B.; Bingi, K.; Prusty, B.R.; Ibrahim, R. Recent advances and applications of spiral dynamics optimization algorithm: A review. *Fractal Fract.* **2022**, *6*, 27. [CrossRef]
12. Agwa, A.; Elsayed, S.; Ahmed, M. Design of Optimal Controllers for Automatic Voltage Regulation Using Archimedes Optimizer. *Intell. Autom. Soft Comput.* **2022**, *31*, 799–815. [CrossRef]
13. Micev, M.; Ćalasan, M.; Radulović, M. Optimal design of real PID plus second-order derivative controller for AVR system. In Proceedings of the 2021 25th International Conference on Information Technology (IT), Zabljak, Montenegro, 16–20 February 2021; pp. 1–4.
14. Ćalasan, M.; Micev, M.; Radulović, M.; Zobaa, A.F.; Hasanien, H.M.; Abdel Aleem, S.H. Optimal PID controllers for avr system considering excitation voltage limitations using hybrid equilibrium optimizer. *Machines* **2021**, *9*, 265. [CrossRef]
15. Micev, M.; Ćalasan, M.; Ali, Z.M.; Hasanien, H.M.; Aleem, S.H.A. Optimal design of automatic voltage regulation controller using hybrid simulated annealing–Manta ray foraging optimization algorithm. *Ain Shams Eng. J.* **2021**, *12*, 641–657. [CrossRef]
16. Chatterjee, S.; Dalel, M.A.; Palavalasa, M. Design of PID plus second order derivative controller for automatic voltage regulator using whale optimizatio algorithm. In Proceedings of the 2019 3rd International Conference on Recent Developments in Control, Automation & Power Engineering (RDCAPE), Noida, India, 10–11 October 2019; pp. 574–579.
17. Sahib, M.A. A novel optimal PID plus second order derivative controller for AVR system. *Eng. Sci. Technol. Int. J.* **2015**, *18*, 194–206. [CrossRef]
18. Moschos, I.; Parisses, C. A novel optimal PIλDND2N2 controller using coyote optimization algorithm for an AVR system. *Eng. Sci. Technol. Int. J.* **2022**, *26*, 100991. [CrossRef]
19. Tabak, A. A novel fractional order PID plus derivative (PIλDμDμ2) controller for AVR system using equilibrium optimizer. *COMPEL Int. J. Comput. Math. Electr. Electron. Eng.* **2021**, *40*, 722–743. [CrossRef]
20. Hossam-Eldin, A.A.; Negm, E.; Ragab, M.; AboRas, K.M. A maiden robust FPIDD2 regulator for frequency-voltage enhancement in a hybrid interconnected power system using Gradient-Based Optimizer. *Alexandria Eng. J.* **2023**, *65*, 103–118. [CrossRef]
21. Priyadarshani, S.; Satapathy, J. Novel Application of Gradient-Based Optimizer for tuning a Fuzzy-PIDD 2 controller for Load Frequency Stabilization. In Proceedings of the 2021 IEEE International Conference on Electronics, Computing and Communication Technologies (CONECCT), Bangalore, India, 8–10 July 2022; pp. 1–6.
22. Khudhair, M.; Ragab, M.; AboRas, K.M.; Abbasy, N.H. Robust control of frequency variations for a multi-area power system in smart grid using a newly wild horse optimized combination of PIDD2 and PD controllers. *Sustainability* **2022**, *14*, 8223. [CrossRef]
23. Kumar, M.; Hote, Y.V. Robust PIDD2 controller design for perturbed load frequency control of an interconnected time-delayed power systems. *IEEE Trans. Control Syst. Technol.* **2020**, *29*, 2662–2669. [CrossRef]
24. Shankar, R. Sine-Cosine algorithm based PIDD 2 controller design for AGC of a multisource power system incorporating GTPP in DG unit. In Proceedings of the 2018 International Conference on Computational and Characterization Techniques in Engineering & Sciences (CCTES), Lucknow, India, 14–15 September 2018; pp. 197–201.
25. Debbarma, S.; Nath, A.; Sarma, U.; Saikia, L.C. Cuckoo search algorithm based two degree of freedom controller for multi-area thermal system. In Proceedings of the 2015 International Conference on Energy, Power and Environment: Towards Sustainable Growth (ICEPE), Shillong, India, 12–13 June 2015; pp. 1–6.
26. Lazarević, M.P.; Mandić, P.D.; Cvetković, B.; Bučanović, L.; Dragović, M. Advanced open-closed-loop PIDD 2/PID type ILC control of a robot arm. In Proceedings of the 2018 Innovations in Intelligent Systems and Applications (INISTA), Thessaloniki, Greece, 3–5 July 2018; pp. 1–8.

27. Todd, C.; Koujan, H.; Fasciani, S. A Hybrid Controller for Inflight Stability and Maneuverability of an Unmanned Aerial Vehicle in Indoor Terrains. *Autom. Control Syst. Eng. J.* **2017**, *17*, 27–39.
28. Izci, D.; Ekinci, S.; Eker, E.; Dündar, A. Assessment of slime mould algorithm based real PID plus second-order derivative controller for magnetic levitation system. In Proceedings of the 2021 5th International Symposium on Multidisciplinary Studies and Innovative Technologies (ISMSIT), Ankara, Turkey, 21–23 October 2021; pp. 6–10.
29. Simanenkov, A. An analysis of PIDD2 controllers optimal adjusting algorithm in mpp fuel preparation system. *EUREKA Phys. Eng.* **2017**, 3–12. [CrossRef]
30. Qiankun, M.; Xuyong, W.; Fan, Y.; Jianfeng, T.; Peng, L. Research on feed-forward PIDD2 control for hydraulic continuous rotation motor electro-hydraulic servo system with long pipeline. In Proceedings of the 2016 UKACC 11th International Conference on Control (CONTROL), Belfast, UK, 31 August–2 September 2016; pp. 1–6.
31. Zhou, K.; Wang, X.; Tao, J.; Guo, X.; Xu, C. Research on a novel PID based controller for nonmagnetic hydraulic navigation simulator with AMESim simulation. In Proceedings of the 2012 UKACC International Conference on Control, Cardiff, UK, 3–5 September 2012; pp. 496–501.
32. Pashchenko, F.; Pikina, G.; Rodomanova, Y. Universal searchless method for parametric optimization of predictive algorithms. In Proceedings of the 2017 13th IEEE International Conference on Control & Automation (ICCA), Ohrid, North Macedonia, 3–6 July 2017; pp. 952–957.
33. Izvoreanu, B.; Cojuhari, I. The Tuning of the PID and PIDD2 Algorithms to the Model Objects with Inertia and Identical Elements and Time Delay. 2013. Available online: http://repository.utm.md/handle/5014/17375 (accessed on 15 July 2023).
34. Alexík, M. Adaptive Self-Tuning PIDD2 Algorithm. *IFAC Proc. Vol.* **2003**, *36*, 83–88. [CrossRef]
35. Huba, M. Extending spectrum of filtered controllers for ipdt plant models. In Proceedings of the 2018 Cybernetics & Informatics (K&I), Lazy pod Makytou, Slovakia, 31 January–3 February 2018; pp. 1–6.
36. Jaradat, M.A.; Sawaqed, L.S.; Alzgool, M.M. Optimization of PIDD2-FLC for blood glucose level using particle swarm optimization with linearly decreasing weight. *Biomed. Signal Process. Control* **2020**, *59*, 101922. [CrossRef]
37. Kumar, M.; Hote, Y.V. PIDD2 Controller Design Based on Internal Model Control Approach for a Non-Ideal DC-DC Boost Converter. In Proceedings of the 2021 IEEE Texas Power and Energy Conference (TPEC), College Station, TX, USA, 2–5 February 2021; pp. 1–6.
38. Bingi, K.; Ibrahim, R.; Karsiti, M.N.; Hassan, S.M.; Harindran, V.R. *Fractional-Order Systems and PID Controllers*; Springer: Berlin/Heidelberg, Germany, 2020; Volume 264.
39. Mystkowski, A.; Zolotas, A. PLC-based discrete fractional-order control design for an industrial-oriented water tank volume system with input delay. *Fract. Calc. Appl. Anal.* **2018**, *21*, 1005–1026. [CrossRef]
40. Lendek, A.; Tan, L. Mitigation of derivative kick using time-varying fractional-order PID control. *IEEE Access* **2021**, *9*, 55974–55987. [CrossRef]
41. Ghamari, S.M.; Narm, H.G.; Mollaee, H. Fractional-order fuzzy PID controller design on buck converter with antlion optimization algorithm. *IET Control Theory Appl.* **2022**, *16*, 340–352. [CrossRef]
42. Bingi, K.; Ibrahim, R.; Karsiti, M.N.; Hassan, S.M. Fractional order set-point weighted PID controller for pH neutralization process using accelerated PSO algorithm. *Arab. J. Sci. Eng.* **2018**, *43*, 2687–2701. [CrossRef]
43. Bingi, K.; Ibrahim, R.; Karsiti, M.N.; Hassam, S.M.; Harindran, V.R. Frequency response based curve fitting approximation of fractional-order PID controllers. *Int. J. Appl. Math. Comput. Sci.* **2019**, *29*, 311–326. [CrossRef]
44. Faieghi, M.R.; Nemati, A. On fractional-order PID design. In *Applications of MATLAB in Science and Engineering*; IntechOpen: London, UK, 2011.
45. Shanmugam, S.K.; Duraisamy, Y.; Ramachandran, M.; Arumugam, S. Mathematical modeling of first order process with dead time using various tuning methods for industrial applications. *Math. Model. Eng.* **2019**, *5*, 1–10. [CrossRef]
46. Bingi, K.; Rajanarayan Prusty, B.; Pal Singh, A. A Review on Fractional-Order Modelling and Control of Robotic Manipulators. *Fractal Fract.* **2023**, *7*, 77. [CrossRef]